Axonal ER Ca^{2+} Release Enhances Miniature, but Reduces Activity-Dependent Glutamate Release in a Huntington Disease Model

James P. Mackay[1], Amy I. Smith-Dijak[1,2], Ellen T. Koch[1,2], Peng Zhang[1], Evan Fung, Wissam B. Nassrallah[1,3], Caodu Buren[1,2], Mandi Schmidt[2,4], Michael R. Hayden[4] and *Lynn A. Raymond[1]

[1] Department of Psychiatry, Djavad Mowafaghian Centre for Brain Health,

[2] Graduate Program in Neuroscience

[3]MD/PhD Program

[4] Centre for Molecular Medicine and Therapeutics, BC Children's Hospital Research Institute

University of British Columbia, Vancouver, British Columbia, Canada

*Correspondence addressed to:

Lynn A. Raymond, MD, PhD

Department of Psychiatry and Djavad Mowafaghian Centre for Brain Health

University of British Columbia

4834-2255 Wesbrook Mall

Vancouver, BC Canada V6T 1Z3

Lynn.raymond@ubc.ca

Abstract

Action potential-independent (miniature) neurotransmission occurs at all chemical synapses, but remains poorly understood, particularly in pathological contexts. Spontaneous release of Ca^{2+} from the axonal endoplasmic reticulum (ER) is thought to facilitated miniature neurotransmission, and aberrant ER Ca^{2+} handling is notably implicated in the progression of Huntington's disease (HD) and other neurodegenerative diseases. Here, we report elevated glutamate-mediated miniature synaptic event frequencies in YAC128 (HD-model) cortical neurons, which pharmacological experiments suggest is mediated by enhanced spontaneous ER Ca^{2+} release. Calcium imaging using an axon-localized sensor revealed slow action potential (AP)-independent axonal Ca^{2+} waves, which were more common in YAC128 cortical neurons. Conversely, spontaneous axonal ER Ca^{2+} release was associated with reduced AP-dependent axonal Ca^{2+} events and consequent glutamate release. Together, our results suggest spontaneous release of axonal ER Ca^{2+} stores oppositely regulates activity-dependent and -independent neurotransmitter release in HD, with potential implications for the fidelity and plasticity of cortical excitatory signaling.

Introduction

Huntington's disease (HD) is a fatal, autosomal dominantly-inherited neurodegenerative disorder caused by a polyglutamine-encoding CAG repeat-expansion (>35 repeats) in exon-1 of the huntingtin gene ("A novel gene containing a trinucleotide repeat that is expanded and unstable on Huntington's disease chromosomes. The Huntington's Disease Collaborative Research Group.,"

49 1993). Disease onset is typically in middle age, characterized by progressively disordered
50 movement and declining cognition (Bachoud-Lévi et al., 2019). Although the mutant huntingtin
51 protein (mHTT) is widely expressed, GABAergic spiny projection neurons (SPN)s of the striatum
52 and pyramidal neurons of the cerebral cortex show the most severe degeneration in HD (Graveland
53 et al., 1985; Vonsattel et al., 1985). Cortical glutamatergic afferents extensively innervate striatal
54 SPNs and dysfunction at these synapses is thought to precede overt neuron loss in HD (Raymond
55 et al., 2011).
56
57 Glutamate-mediated toxicity was initially proposed to contribute to pathogenesis in HD based on
58 studies showing that striatal injections of glutamate receptor agonists largely recapitulate HD
59 pathology in animals (Beal et al., 1986; Hantraye et al., 1990). More recently, studies in SPNs
60 from transgenic and knock-in mouse models of HD demonstrate enhanced extrasynaptic N-
61 Methyl-D-Aspartate receptor (NMDAR) surface expression and function that may explain, in part,
62 increased susceptibility to excitotoxic challenges (Botelho et al., 2014; Fan et al., 2007; Kovalenko
63 et al., 2018; Milnerwood et al., 2010; Plotkin et al., 2014; Zeron et al., 2002). Cell stress/death
64 signaling mediated by elevated levels of extrasynaptic NMDARs in HD SPNs may be further
65 exacerbated by reduced glutamate transporter function (Miller et al., 2008), although recent studies
66 show glutamate clearance after synaptic release is normal or accelerated in striatal and cortical
67 brain slice (Parsons et al., 2016). Additionally, some studies show synaptic glutamate release from
68 cortical afferents is altered in HD mouse models, possibly contributing to excitotoxicity and
69 synaptic dysfunction (Cepeda et al., 2003; Joshi et al., 2009; Raymond et al., 2011). However, the
70 direction of this effect appears to be model and disease-stage dependent; relative to wildtype (WT),

71 glutamate release is typically enhanced early, but reduced with disease progression in HD mice
72 (Joshi et al., 2009).
73
74 Mutant HTT (mHTT) directly interacts with endoplasmic reticulum (ER) type-1 inositol (1,4,5)-
75 triphosphate receptors (IP3Rs) sensitizing their Ca^{2+} release in response to IP3 (Tang et al., 2003);
76 blocking this interaction normalizes IP3-induced ER Ca^{2+} release *in vitro* and improves behavioral
77 outcomes in HD-model mice (Tang et al., 2009). Furthermore, evidence suggests Ryanodine
78 receptors, which are ER-localized Ca^{2+} channels that mediate Ca^{2+}-induced Ca^{2+} release, are
79 constitutively leaky in HD mouse models (Suzuki et al., 2012). Although these studies focused on
80 the soma and dendrites of SPNs at the postsynaptic side of cortical-striatal synapses, ER is found
81 in all neuronal compartments, including presynaptic terminals, where its Ca^{2+} stores, when
82 released, modulate neurotransmission (Emptage et al., 2001; Llano et al., 2000). However, it is
83 unknown whether presynaptic ER Ca^{2+} handling is also dysfunctional in HD and if such a process
84 contributes to altered glutamate release from cortical synaptic terminals.
85
86 Here, we have investigated whether glutamate release is altered, and if ER Ca^{2+} dysregulation
87 contributes to aberrant function, in presynaptic terminals of cortical pyramidal neurons from
88 premanifest HD-model mice expressing full-length mHTT with 128 CAG-repeats in a yeast
89 artificial chromosome (YAC128). Our results from neuronal cultures and acute cortical-striatal
90 brain slices demonstrate a shift in balance favoring increased action potential (AP)-independent
91 (miniature) vs. AP-dependent glutamate release, and that altered ER Ca^{2+} release contributes to
92 this change. This may have important previously unidentified disease implications, given the
93 distinct physiologically relevant signaling potentially mediated by miniature neurotransmission

94 (Fishbein and Segal, 2007; Kavalali, 2015). Ultimately our data contribute to growing evidence
95 for cortex and striatal synaptic dysfunction in HD, and support a key role for ER Ca^{2+} dysregulation
96 in this pathophysiology.
97
98 **Results**
99
100 **Mini EPSC frequencies are elevated in YAC128 cortical cultures at early time points**
101
102 Our group previously recorded miniature excitatory post synaptic currents (mEPSCs) from striatal
103 spiny projection neurons (SPNs) co-cultured with cortical neurons from prenatal WT or yeast
104 artificial chromosome (YAC128) mice. YAC128 SPNs showed elevated mEPSC frequencies,
105 compared to WT, at day in vitro (DIV) 14 – a time point when SPN dendritic arborization patterns
106 and spine numbers were similar between genotypes (Buren et al., 2016). At DIV21, YAC128 SPNs
107 showed a significant reduction in total dendritic length, and therefore reduced total excitatory
108 synapse numbers, compared to WT. Despite this, mEPSC frequencies onto WT and YAC128 SPNs
109 were comparable at DIV21.
110
111 The above results suggested a higher rate of action potential-independent glutamate release from
112 YAC128 presynaptic cortical pyramidal neuron (CPN) terminals onto individual SPN synapses.
113 Here, we capitalize on a relatively simpler culture preparation containing only cortex-derived
114 neurons and YAC128 mouse-derived brain slices to mechanistically dissect how mutant huntingtin
115 protein expression affects action potential-independent and -dependent glutamate release from
116 CPN terminals.

117

118 To establish whether miniature glutamate release is enhanced at YAC128 CPN terminals targeting
119 other CPNs, we first established WT and YAC128 CPN mEPSC parameters in cortical cultures at
120 various DIV ages (7, 14, 18 and 21). In general, both genotypes showed increased mEPSC
121 frequencies with culture time. However, YAC128 CPN mEPSC frequencies were consistently
122 higher than age-matched WT controls after DIV7 and up until DIV21, at which point mEPSC
123 frequencies became comparable between genotypes **(Figure 1),** as was also the case in the co-
124 culture model (Buren et al., 2016). The greatest genotype mEPSC frequency difference occurred
125 at DIV14, when mean YAC128 CPN frequencies were more than double that of WT: 10.83 ± 1.80
126 Hz vs 4.52 ± 0.60 Hz, respectively **(Figure 1D, E)**. YAC128 mEPSC frequencies remained
127 significantly higher than WT at DIV18: 14.07 ± 1.54 Hz vs 9.92 ± 1.54 Hz, respectively **(Figure**
128 **1G, H)**. Age matched YAC128 and WT CPNs showed similar mEPSC amplitudes across all DIV
129 time points examined **(Figure 1 C, F, I and L)**. We chose to perform subsequent experiments
130 probing the mechanistic details underlying increased cortical mini glutamate release in DIV18
131 cortical monocultures, since this was the most mature culture stage at which mEPSC frequencies
132 were elevated in YAC128 CPNs.

133

134 **Synapse numbers and dendritic complexity are similar in WT and YAC128 cortical**
135 **pyramidal neurons at DIV 18**

136

137 The higher mEPSC frequencies seen in DIV18 YAC128 CPNs suggest an increased presynaptic
138 glutamate release probability. However, relative differences in synapse numbers could also
139 account for this finding. To estimate numbers of synapses, we first expressed cytosolic GFP in a

140 small proportion of neurons in WT and YAC128 cortical cultures and imaged full CPN dendritic
141 arbors at DIV18. Sholl analysis revealed similar arborization patterns and total dendritic length in
142 WT and YAC128 CPNs **(Supplemental Figure 1A, C)**. In separate cultures, we expressed an
143 internal GFP-tagged anti-PSD95 antibody (Gross et al., 2013) in a subset of neurons and immuno-
144 stained for VGlut1, to identify glutamatergic terminals, and the GluA2 AMPA receptor subunit,
145 to identify functional synapses. Functional synapse numbers, defined as GFP-labeled PSD95
146 puncta colocalized with VGlut1 and GluA2 immunofluorescent-labeled puncta, were not
147 significantly different between DIV18 WT and YAC128 CPNs, although there was a trend towards
148 lower synapse density in YAC128 CPNs **(Supplemental Figure 1E, F)**. Together with the above
149 data showing increased mEPSC frequency in YAC128 CPNs at DIV18 **(Figure 1)**, these results
150 point to an increase in miniature vesicular glutamate release from cortical terminals in YAC128
151 cultures.
152
153 **Releasing ER calcium with low dose ryanodine or caffeine increases the miniature EPSC**
154 **frequency in WT, but not YAC128 cultures**
155
156 Studies using mouse models suggest Ca^{2+} release from ER stores is aberrant in HD due to increased
157 IP3 and ryanodine receptor activity (Suzuki et al., 2012; Tang et al., 2003). Although effects of
158 mHTT on the presynaptic ER have not been specifically studied, we hypothesized a presynaptic
159 ER leak elevates cytosolic Ca^{2+}, thereby mediating the increased miniature glutamate release seen
160 in our YAC128 cultures **(Figure 2A, B)**. To test this hypothesis, we first recorded mEPSCs before
161 and during local application of low dose (5 μM) ryanodine to cultured CPNs; 5 μM ryanodine
162 releases ER Ca^{2+} by opening ryanodine receptors (Meissner, 2017). In WT cultures, 5 μM

163 ryanodine nearly doubled the CPN mEPSC frequency: from 6.74 ± 1.17 Hz to 11.91 ± 2.36 Hz
164 [Students' paired T-test; p=0.0280; n=13 cells] **(Figure 2C - E)**. In YAC128 cultures, however,
165 ryanodine (5 μM) did not significantly alter the CPN mEPSC frequency: 11.98 ± 1.66 Hz vs 13.89
166 ± 2.01 Hz - under control conditions and in ryanodine (5 μM) respectively **(Figure 2F - H)**. A
167 Comparison of the percent change in mEPSC frequency following ryanodine (5 μM) revealed a
168 significantly greater response in WT than in YAC128 CPNs [31.7 ± 7.5 % (n=13) vs 5.2 ± 9.5 %
169 (n=15) in WT and YAC128 CPNs respectively (Students' unpaired T-test; p=0.0418)]. We next
170 used caffeine (1 mM) as an alternative means of agonizing ryanodine receptors; this more
171 prominently increased the mEPSC frequency in WT cultures, but otherwise produced similar
172 results **(Supplemental Figure 2)**.
173
174 **Removing extracellular Ca^{2+} and blocking the ER SERCA pump substantially reduces the**
175 **mEPSC frequency in YAC128 but not WT cultures**
176
177 If an ongoing release of presynaptic ER Ca^{2+} in YAC128 cultures occludes potentiation of synaptic
178 glutamate release by low dose ryanodine and caffeine, blocking ER Ca^{2+} release should reduce
179 synaptic glutamate release in YAC128 cultures. To test this, we pre-incubated cultures with
180 extracellular fluid (ECF) containing the sarco/endoplasmic reticulum Ca^{2+}-ATPase (SERCA)
181 pump inhibitor cyclopiazonic acid (CPA) (30 μM) to deplete ER Ca^{2+} stores. Since ER Ca^{2+}
182 depletion can increase cytosolic Ca^{2+} by engaging the store operated Ca^{2+} response, and this effect
183 can increase mini neurotransmitter release (Emptage et al., 2001), we performed these experiments
184 in the absence of extracellular Ca^{2+}. Under these conditions, YAC128 CPNs showed a mean
185 mEPSC frequency of 3.33 ± 0.57 Hz (n=14), significantly lower than seen in WT CPNs under

186 identical conditions 8.41 ± 1.50 Hz (n=17) (Student's unpaired t-test; p=0.0062) **(Figure 2I-K)**.
187 These results suggest that an ER calcium leak into the cytoplasm elevates mini vesicular glutamate
188 release from YAC128 CPN terminals, and that in the absence of this effect, the intrinsic vesicular
189 release probability is actually reduced in YAC128 compared to WT cortical terminals.
190
191 **Presynaptic Ca^{2+} sparks and waves are more frequent in YAC128 cultures**
192
193 To directly monitor presynaptic Ca^{2+} dynamics, we next fused GCaMP6-M (Chen et al., 2013)
194 with the rat synaptophysin protein via a small glycine-serine linker to generate a genetically-
195 encoded Ca^{2+} sensor that preferentially localizes to presynaptic terminals. We expressed this rat
196 synaptophysin-tagged GCaMP6-M construct (rSyph-GCaMP6m) in neurons in cortical cultures
197 and performed Ca^{2+} imaging experiments, first in the presence of TTX (500 nM) to relate
198 presynaptic Ca^{2+} signaling to our mEPSC findings (above). Remarkably, both YAC128 and WT
199 cultures showed spontaneous axonal Ca^{2+} sparks, often beginning in single boutons, then initiating
200 slow Ca^{2+} waves spreading to neighboring boutons **(Figure 3A, B)**. In some cases, the above waves
201 slowly traversed axons encompassing entire 63X (178.6 μm x 113.1 μm) imaging fields over
202 multiple seconds of imaging. Conversely, axonal Ca^{2+} events in the absence of TTX could not be
203 temporally resolved (owing to relatively slow GCaMP kinetics) and appeared simultaneously
204 across all the boutons of a given imaged axon. These mini presynaptic Ca^{2+} events in TTX were
205 also strikingly long lasting at individual boutons - on average 5 - 10 times longer than that of
206 typical events seen in the absence of TTX **(Figure 3C, D)**. These miniature presynaptic Ca^{2+} events
207 in TTX were more than three times as frequent in YAC128 cultures than in WT cultures **(Figure**
208 **3E)**, but event DF/F amplitudes did not significantly differ between genotypes **(Figure 3F)**. The

209 detection algorithm used here (see methods) considered Ca^{2+} waves involving multiple axonal
210 boutons as single events (as in **Figure 3A**). However, the mean event area was similar in both
211 genotypes (not illustrated), suggesting similar numbers of axonal boutons were recruited on
212 average by such events in YAC128 and WT cultures. In subsets of WT and YAC128 cultures we
213 also expressed an mCherry-tagged PSD95 construct. In these cultures, we repeatedly observed
214 clear colocalizations between rSyph-GCaMP6m-labeled boutons, spontaneously active in TTX,
215 and mCherry-labeled dendritic spines (not illustrated). Thus although we cannot be certain that all
216 boutons showing spontaneous Ca^{2+} events in TTX participate in synaptic connections, it is clear
217 that such events are not restricted to ectopic boutons.
218
219 **Basal cytosolic Ca^{2+} is higher in YAC128 presynaptic boutons**
220
221 In a subset of TTX experiments, we applied the Ca^{2+} ionophore ionomycin (10 μM) to cultures
222 following GCaMP imaging. By equilibrating cytosolic Ca^{2+} to extracellular levels, this approach
223 allowed quantification of GCaMP fluorescence in the presence of the known extracellular Ca^{2+}
224 concentration (here 2 mM). Thus, smaller ionomycin-mediated increases in GCaMP fluorescence
225 indicate relatively higher basal (pre-ionomycin) cytosolic Ca^{2+} concentrations (Lindhout et al.,
226 2019). In both genotypes, ionomycin-mediated changes in presynaptic GCaMP fluorescence
227 (DF/F) were significantly smaller in boutons that had shown at least one spontaneous Ca^{2+} event
228 in the previous 3 min recording **(Figure 4A, D)**, indicating higher basal cytosolic Ca^{2+}
229 concentrations in these spontaneously active boutons. Furthermore, overall ionomycin responses
230 were significantly smaller in YAC128 cultures than in WT cultures when comparing the entire
231 population of boutons imaged in a culture (both spontaneously active and inactive) **(Figure 4E)**.

232

233 **Caffeine increases basal Ca^{2+} and miniature events in WT, but not YAC128 cortical boutons**

234

235 The slow kinetics of the above miniature presynaptic Ca^{2+} events are consistent with ER-mediated
236 Ca^{2+} waves reported in postsynaptic neuronal compartments (Ross, 2012). We next tested whether
237 these presynaptic Ca^{2+} events were affected by caffeine (1 mM), an ER ryanodine receptor agonist
238 that substantially increased mEPSC frequencies in WT, but not YAC128 cultures (above). In the
239 presence of TTX, caffeine (1 mM) significantly increased the presynaptic Ca^{2+} event frequency in
240 WT cultures **(Figure 5A)**, but did not significantly alter event frequency in YAC128 cultures
241 **(Figure 5B)**.

242

243 Significant photobleaching of the rSyph-GCaMP6m construct occurred with prolonged imaging;
244 this combined with the relative infrequency of mini presynaptic Ca^{2+} events necessitated imaging
245 of separate fields for the above control and caffeine comparisons. We next performed within-
246 bouton measurements of basal rSyph-GCaMP6m fluorescence before and immediately following
247 application of caffeine; the relatively short duration of these experiments made before and after
248 measurements feasible. A clear slow increase in basal rSyph-GCaMP6m fluorescence was seen in
249 most WT boutons following caffeine (1 mM) application **(Figure 5C)**, which was generally absent
250 or reduced in YAC128 boutons **(Figure 5D)**. Overall a significantly greater caffeine (1 mM)-
251 mediated increase in rSyph-GCaMP6m fluorescence was seen in WT boutons compared to
252 YAC128 **(Figure 5E)**.

253

254

255 **Action potential-dependent Ca^{2+} signals in presynaptic cortical terminals Are less frequent**
256 **in YAC128 cultures**
257
258 We next used the rSyph-GCaMP6m construct in the absence of TTX to examine presynaptic action
259 potential-dependent Ca^{2+} signals in WT and YAC128 cortical cultures. When neuronal action
260 potential firing was intact, rSyph-GCaMP6m -expressing boutons in both WT and YAC128
261 cultures were dominated by presumably voltage-gated Ca^{2+} channel-mediated signals **(Figure 6A,**
262 **B)**. These signals were more frequent than those seen in the presence of TTX, but of far shorter
263 duration. Interestingly, these activity-dependent Ca^{2+} events were nearly twice as frequent in WT
264 axonal boutons, compared to those in YAC128 cultures **(Figure 6A, C and E).** Ryanodine (5 μM)
265 modestly but significantly reduced the frequency of these events in WT cultures (by 17 %) **(Figure**
266 **6A, B and E)**. Conversely, 5 μM ryanodine elicited a modest, but significant increase in the
267 frequency of these events in YAC128 cultures **(Figure 6C- E)**.
268
269 As discussed above, rSyph-GCaMP6m events in the presence of TTX were typically much longer
270 in duration than action potential-dependent events in both genotypes and appeared to be restricted
271 to a subset of boutons with higher resting Ca^{2+} concentrations. Interestingly, similar strikingly
272 long-lasting events continued to occur in subsets of boutons in the absence of TTX. In an attempt
273 to identify boutons exhibiting these slow Ca^{2+} events, we next categorized boutons imaged in the
274 absence of TTX based on whether one or more Ca^{2+} events with a duration greater than 6 s
275 (measured at half peak amplitude) occurred during a 3 min recording. 6 s was chosen as the cutoff
276 value, because it was more than 5 standard deviations greater than the mean event duration seen
277 in WT and YAC128 boutons in the absence of TTX, but comparable to average event durations in

278 TTX in both genotypes: [8.60 ± 0.92 s (n=164) and 6.23 ± 0.35 s (n=440) in WT and YAC128
279 boutons respectively]. Without TTX, 7.9 % (23/292) of WT boutons showed one or more events
280 lasting longer than 6 s, while under identical conditions 10.4 % (44/423) of YAC128 boutons
281 showed at least one such event. Interestingly in both genotypes, overall event frequencies were
282 significantly lower in boutons showing one or more slow events (>6 s) than in boutons showing
283 only short duration events **(Figure 6F- I)**. Assuming boutons displaying these long lasting Ca^{2+}
284 events correspond to the same population that is spontaneously active in TTX, these results suggest
285 action potential-dependent Ca^{2+} events are reduced in the bouton population with higher resting
286 cytosolic Ca^{2+} levels and spontaneous ER release events. Taken together, experiments up to this
287 point suggest that releasing presynaptic ER Ca^{2+} elevates miniature vesicular glutamate release,
288 but can also reduce activity-dependent presynaptic Ca^{2+} influx, and imply that the spontaneous or
289 pharmacological release of presynaptic ER Ca^{2+} oppositely regulates miniature and action
290 potential-dependent glutamate release.
291
292 **Low dose ryanodine reduces evoked glutamate release in WT- but not YAC128-derived**
293 **brain slices**
294
295 We next performed experiments in cortical-striatal *ex-vivo* brain slices prepared from 2 – 3 month
296 old WT and YAC128 mice expressing the fluorescent glutamate sensor iGluSnFR in striatal
297 neurons (Parsons et al. 2016; Koch et al. 2018). This preparation allowed direct optical
298 measurement of glutamate release in the striatum, independent of postsynaptic neuronal properties.
299 Striatal iGluSnFR signals evoked by stimulating cortical axons of the corpus callosum were
300 significantly decreased by ryanodine (5 μM) in WT, but not YAC128 slices **(Figure 7)**. These data

301 are consistent with results in culture (Figs. 6), suggesting that AP-dependent glutamate release is
302 reduced in YAC128 as a consequence of a tonic Ca^{2+} leak from ER stores
303
304 **Discussion**
305
306 Presynaptic neurotransmitter release and consequent postsynaptic signaling largely underlies
307 communication between neurons, thus forming the basis of brain circuitry. Neurotransmitter
308 release in turn, can be broadly divided into action potential-dependent or independent forms. The
309 former requires presynaptic voltage-gated Ca^{2+} channel activation coordinated by sodium action
310 potentials; while the latter persists in the absence of neuronal activity. Although miniature
311 neurotransmission is poorly understood compared to its activity-dependent counterpart, it is
312 increasingly accepted to subserve clear physiological functions (Frank et al., 2006; McKinney et
313 al., 1999; Sutton et al., 2006). Moreover, miniature release can be regulated relatively
314 independently of action potential-dependent release and may even be mediated by distinct
315 vesicular pools (Fredj and Burrone, 2009; Sara et al., 2005).
316
317 Alterations in synaptic signaling processes, particularly relating to the excitatory transmitter
318 glutamate, have been repeatedly reported in models of HD (Raymond et al., 2011; Sepers et al.,
319 2017; Tyebji and Hannan, 2017) and other neurodegenerative diseases (R. Wang and Reddy,
320 2017). Increased cell-surface expression of extra-synaptic NMDA receptors by SPNs favors
321 excitotoxic postsynaptic glutamate-mediated signaling in HD models (Milnerwood et al., 2010).
322 Mounting evidence also suggests glutamate release from cortical afferents is altered in HD;

323 however, the direction of this alteration appears to be disease-stage-dependent (Cepeda et al.,
324 2003; Joshi et al., 2009).
325
326 The endoplasmic reticulum (ER), a continuous intracellular membrane-system involved in Ca^{2+}
327 storage and protein synthesis, is expressed in all neuronal processes including axons and
328 presynaptic boutons. Increased cytosolic Ca^{2+}-release from the ER has been shown in HD models,
329 as a result of a mutant huntingtin protein (mHTT)-mediated increase in IP3 receptor
330 responsiveness (Tang et al., 2003) and a constituent ryanodine receptor Ca^{2+} leak (Suzuki et al.,
331 2012). Previous HD studies have focused on the postsynaptic ER, however Ca^{2+} release from the
332 presynaptic ER is known to modulate neurotransmitter release (Emptage et al., 2001; Llano et al.,
333 2000). Results of our study suggest mHTT expression alters ER Ca^{2+} handling at stores in close
334 proximity to cortical presynaptic terminals, thereby altering glutamate release. This mechanism
335 clearly increased the frequency of Ca^{2+}-dependent, action potential-independent (mini) synaptic
336 glutamate events in our YAC128 model. Conversely, our findings suggest reduced action
337 potential-dependent glutamate release from YAC128 cortical terminals. As we have focused
338 exclusively on glutamatergic synapses, future experiments will be required to determine if this
339 mechanism similarly affects the release of other neurotransmitters and neuromodulators.
340
341
342 **Spontaneous axonal Ca^{2+} signaling increases the YAC128 miniature glutamate release**
343 **frequency**
344

345 CPNs in YAC128 cortical cultures at DIV14 and DIV18 showed higher mEPSCs frequencies
346 compared to CPNs in age-matched WT cultures. However by DIV 21, mEPSC frequencies were
347 similar between WT and YAC128 CPNs. This pattern is reminiscent of SPN mEPSC frequencies
348 in YAC128 cortical-striatal co-cultures, which were also higher relative to WT at early DIV ages,
349 but comparable to WT by DIV21 (Buren et al., 2016). In the co-culture model, the total dendritic
350 length of YAC128 SPNs was reduced relative to WT at DIV21, indicating reduced total SPN
351 synapse numbers may have masked ongoing elevated glutamate release rates from individual
352 YAC128 cortical terminals. We suspect that in our cortical cultures, degenerative changes at
353 DIV21 likewise obscured the elevated YAC128 CPN mEPSC frequencies clearly seen at earlier
354 DIV ages. Notably in DIV18-aged cortical cultures, the time point at which we performed
355 mechanistic experiments, no genotype differences in CPN synapse density and dendritic
356 morphology were evident, indicating that differences in mEPSC frequencies likely reflected
357 altered rates of release at individual presynaptic sites. In any case, increased rates of miniature
358 glutamate release appear to be an early and perhaps enduring phenotype of cultured YAC128
359 CPNs.
360
361 Caffeine or low dose ryanodine, which release ER Ca^{2+} by opening ryanodine receptors, failed to
362 increase the mEPSC frequency in YAC128 CPNs, despite robustly increasing the WT mEPSC
363 frequency. This result, in concert with the increased basal YAC128 mEPSC frequency, suggests
364 an ongoing spontaneous Ca^{2+} store release in YAC128 cultures occludes facilitation of the mEPSC
365 frequency by drug-mediated Ca^{2+} store release. The substantially lower CPN mEPSC frequency
366 seen in YAC128 cultures incubated with the ER SERCA pump inhibitor CPA in nominally zero
367 extracellular Ca^{2+}, is also consistent with a strong ER-derived Ca^{2+}-dependence of YAC128 mini

368 glutamate release. Conversely, mEPSC frequencies in WT cultures were not substantially reduced
369 under identical conditions; this resulted in significantly higher WT than YAC128 mEPSC
370 frequencies in CPA and 0 mM extracellular Ca^{2+}, notably opposite the relationship seen without
371 CPA in standard (2 mM) extracellular Ca^{2+}. This was unexpected given overall WT and YAC128
372 CPN synapse numbers were similar in these cultures, but may indicate a reduction in functional
373 YAC128 synapses, not apparent in fixed culture images, or deficits in the YAC128 synaptic release
374 machinery, as suggested in previous studies (Morton and Edwardson, 2001; Morton et al., 2001).
375 In either case, enhanced Ca^{2+}-dependent mini glutamate release in YAC128 cultures clearly
376 surmounts any such deficits. These results also suggest mini glutamate release in WT cultures is
377 largely Ca^{2+}-independent. In contrast, Xu et. al (2009) reported mini glutamate release in similar
378 cortical cultures persisted in the absence of extracellular Ca^{2+}, but was nearly completely
379 dependent on internal Ca^{2+}stores and blocked by preincubation with the membrane-permeant Ca^{2+}
380 chelator BAPTA-AM (Xu et al., 2009). If this were true in our cultures, we would expect Ca^{2+}
381 store depletion (with CPA), in concert with removal of extracellular Ca^{2+}, to similarly abolish mini
382 release. However CPA is reported to only partially deplete presynaptic ER Ca^{2+} (de Juan-Sanz et
383 al., 2017), therefore a role of residual ER Ca^{2+} in maintaining mini release in WT cultures under
384 these conditions cannot be excluded.
385
386 Despite a clear role of ER Ca^{2+} in mini release in a variety of neuronal preparations, the temporal
387 and spatial dynamics of action potential-independent presynaptic ER Ca^{2+} signals are largely
388 unclear. Imaging the rSyph-GCaMP6m probe in TTX revealed spontaneous, presynaptic Ca^{2+}
389 events that often initiated Ca^{2+} waves traversing cortical axons. These events were more frequent
390 in YAC128 cultures and showed strikingly slow kinetics in both genotypes, consistent with ER

391 Ca^{2+} waves reported in dendrites and non-neuronal cell-types (Ross, 2012). Caffeine substantially
392 increased the mini axonal Ca^{2+} event frequency in WT cultures to levels comparable to that seen
393 in YAC128 cultures, but failed to significantly change the event frequency in YAC128 cultures.
394 The congruence of these results with our mEPSC findings (above) suggests these axonal Ca^{2+}
395 events underlie the increased YAC128 mini glutamate release frequencies.
396
397 Basal cytosolic Ca^{2+} concentrations were higher in axonal boutons showing spontaneous Ca^{2+}
398 activity in TTX, compared to inactive boutons, in both genotypes. Elevated cytosolic Ca^{2+} levels
399 may therefore be required to precipitate the initial ryanodine or IP3 receptor opening needed to
400 incite the regenerative ER Ca^{2+}-induced Ca^{2+} release we presume underlie these axonal Ca^{2+}
401 events. Interestingly, the restriction of spontaneous Ca^{2+} signals to a subset of cortical boutons
402 with higher basal Ca^{2+} concentrations may mean mini glutamate release is not uniform across
403 cortical boutons, but favored from this population of spontaneously active boutons. Indeed,
404 subpopulations of synaptic boutons favoring mini release have been described in other neuronal
405 systems (Atasoy et al., 2008; Peled et al., 2014). We suspect the higher basal cytosolic Ca^{2+}
406 concentrations in the overall YAC128 axonal bouton population meant a greater proportion were
407 capable of sustaining spontaneous Ca^{2+} activity. Caffeine application increased the baseline
408 cytosolic Ca^{2+} concentration and frequency of spontaneous events in WT, but not YAC128
409 boutons, consistent with this idea.
410
411
412
413

414 **Action potential-dependent glutamate release is suppressed due to presynaptic ER depletion**

415

416 Regardless of genotype, striking differences were seen in the rSyph-GCaMP6m signals that
417 predominated in the presence versus absence of TTX. Most rSyph-GCaMP6m-expressing boutons
418 in the absence of TTX showed numerous spontaneous events during standard 3 min imaging
419 sessions. However, only subsets of boutons were spontaneously active in TTX, with active boutons
420 characterized by higher resting cytosolic Ca^{2+} concentrations. Furthermore, although Ca^{2+} events
421 at individual boutons in TTX were less frequent, they lasted many times longer than corresponding
422 action potential-dependent events. Interestingly in the absence of TTX, subsets of boutons of both
423 genotypes showed longer-lasting Ca^{2+} events, like those that persisted in TTX, typically alongside
424 faster action potential-dependent events. We suspect these boutons correspond to the population
425 spontaneously active in TTX. Event frequencies in such boutons, in the absence of TTX, were
426 significantly lower than in boutons lacking these longer-lasting events, further supporting the idea
427 that subsets of cortical boutons favor either miniature or action potential-dependent glutamate
428 release.

429

430 Although spontaneous axonal Ca^{2+} events were more common in YAC128 cultures in the presence
431 of TTX, the opposite was true when experiments were performed without TTX, suggesting
432 reduced activity-dependent glutamate release in YAC128 cultures. Reduced action potential-
433 dependent axonal Ca^{2+} event frequencies in YAC128 cultures could reflect decreased CPN firing
434 rates, altered transduction of sodium action potentials to bouton Ca^{2+} signals or some combination
435 of these factors. 5 μM ryanodine significantly reduced the frequency of these action potential-
436 dependent bouton Ca^{2+} events in WT cultures, though not to YAC128 levels, consistent with

437 reduced action potential-dependent presynaptic Ca^{2+} signaling in YAC128 cultures being partly,
438 but not entirely mediated, by spontaneous release of ER Ca^{2+}. However, nuances of ryanodine's
439 pharmacology may have confounded this conclusion. Low dose ryanodine opens ryanodine
440 receptors, but to a sub-maximal conductance state. Furthermore, ryanodine binding to a second
441 low affinity receptor site mediates channel closure, an action that predominates at doses greater
442 than 10 μM. Caffeine more effectively releases ER Ca^{2+}, exemplified here in patch clamp mini
443 EPSC experiments, and may therefore have been capable of lowering action potential-dependent
444 event frequencies in WT to YAC128 levels. Unfortunately, caffeine was undesirable for these
445 experiments because, unlike ryanodine, it is an antagonist at adenosine receptors, which are often
446 expressed at presynaptic sites and inhibit VGCCs (Dunwiddie and Masino, 2001). We speculate
447 that the ryanodine receptor population in YAC128 boutons favors the open conformation under
448 basal conditions, consistent with the lack of caffeine responses in YAC128 boutons, and that under
449 such conditions, ryanodine-mediated channel closure would be exaggerated. If so, this could
450 account for the modest, but significant ryanodine-mediated increase in event frequencies in
451 YAC128 boutons.
452
453 Precise mechanism(s) by which pharmacological or disease-mediated ER Ca^{2+} release might
454 reduce activity-dependent presynaptic Ca^{2+} signaling remain uncertain. Indeed axonal or cell body
455 ER stores could equally underlie this effect given the dependence of these signals on sodium action
456 potentials. Dendritic ryanodine receptor activation has been shown to reduce neuronal firing rates
457 via activation of a Ca^{2+}-dependent K^+ conductance (van de Vrede et al., 2007). Alternatively,
458 elevated cytosolic Ca^{2+} levels in YAC128 boutons (mediated by the release of axonal stores) might
459 contribute to Ca^{2+}-dependent VGCC inactivation, thereby reducing the coupling of cortical action

460 potentials to presynaptic VGCC-mediated Ca^{2+} influx. Indeed, more generalized increases in
461 cytosolic Ca^{2+} mediated by ER store release, have been shown to facilitate Ca^{2+}-dependent
462 inactivation of voltage-gated Ca^{2+} channels including the N and P/Q-types commonly expressed
463 in presynaptic terminals and implicated in vesicular release (Budde et al., 2002; Cens et al., 2006).
464 If this were the case in our system, the higher resting Ca^{2+} concentrations evident in YAC128
465 boutons would be expected to maintain local voltage-gated Ca^{2+} channels in a higher resting state
466 of inactivation.
467
468 Low-dose ryanodine decreased the amplitude of striatum, glutamate-mediated iGluSnFR signals
469 in WT brain slices, an effect absent or diminished in YAC128 slices, consistent with our findings
470 in culture. There is a lack of consensus as to whether single action potentials can trigger Ca^{2+}-
471 induced Ca^{2+} release from the presynaptic ER (Emptage et al., 2001), or whether prolonged,
472 repetitive action potential firing is required (de Juan-Sanz et al., 2017). It seems unlikely that the
473 stimulation protocol used here appreciably contributed to the action potential-dependent discharge
474 of the presynaptic ER, given the relatively low intensity stimulation used (repeated only twice at
475 100 Hz). Rather, we suspect a ryanodine-mediated increase in presynaptic Ca^{2+} decreased evoked
476 glutamate release by inactivating presynaptic voltage-gated Ca^{2+} channels in WT slices, and that
477 this process was occluded in YAC128 slices. However, future studies will be required to clarify
478 mechanistic details of this process.
479
480 Taken together, the evidence presented here strongly suggests enhanced spontaneous release of
481 presynaptic ER Ca^{2+} in YAC128 mice favors miniature glutamate release at the expense of evoked
482 release.

483

484 **Implications for postsynaptic signaling**

485 Mini glutamate release elicits postsynaptic NMDA receptor-mediated Ca^{2+} influx under
486 physiologically relevant conditions (Beaulieu-Laroche and Harnett, 2018; Espinosa and Kavalali,
487 2009) and can mediate postsynaptic signaling distinct from that of action potential-dependent
488 release (Sutton et al., 2007). Indeed mini glutamate release may activate distinct populations of
489 NMDAR receptors (Atasoy et al., 2008). In cultures, it was reported that miniature glutamate-
490 mediated events become toxic to CPNs following prolonged silencing of neuronal activity with
491 TTX (Fishbein and Segal, 2007). Future studies will be necessary to determine if and how the
492 increased mini glutamate release shown here interacts with the well described alterations in
493 postsynaptic NMDA receptor expression in the YAC128 and other HD-models, and whether a
494 shift towards activity-independent glutamate release contributes to neurodegeneration in HD.

495

496 **Materials and Methods**

497

498 **Culture preparation:**

499 All animal-related procedures were approved by and adhered to the guidelines of the University
500 of British Columbia Committee on Animal Care and the Canadian Council on Animal Care
501 (protocols A17-0295, A15-0069 and A19-0076). Cultures were prepared from both male and
502 female embryonic day 17-18 pups from either wild-type (WT) FVB/N or transgenic yeast artificial
503 chromosome-containing mice expressing the full-length human huntingtin genomic DNA with 128
504 CAG repeats (YAC128). YAC128 mice were maintained on the FVB/N background (homozygous
505 line 55). Wildtype and YAC128 mice used for ex vivo slice experiments (below) and bred for

506 culture preparation (above) were group housed under controlled conditions, free of know
507 pathogens, at room temperature (22 – 24 °C), under a 12 hr light/dark cycle. Cortical cultures used
508 in patch clamp electrophysiology and Ca^{2+}-imaging experiments were prepared as previously
509 described (Milnerwood et al., 2012; Smith-Dijak et al., 2019) and plated at a density of 225, 000
510 neurons/ml. In a subsets of experiments, a portion of the total 2.7 million cortical neurons (plated
511 per 24-well culture) were transfected with transgenic reporters including: GFP; a synaptophysin-
512 tagged GCaMP6-M construct (a generous gift from Dr. Anne Marie Craig, UBC); a postsynaptic
513 density 95 (PSD-95)–tagged M-cherry construct; or a GFP-tagged internally expressed anti-
514 PSD95 antibody (a generous gift from Dr. D.B. Arnold, University of Southern California; (Gross
515 et al., 2013)).
516
517 **Electrophysiology:**
518 An Axopatch 200B amplifier and pClamp 9.2 software (Molecular Devices, Sunnyvale, CA) were
519 used to acquire whole-cell patch clamp electrophysiology recordings. Data was digitized at 20 kHz
520 and low-pass filtered at 1 kHz. For electrophysiology experiments, cultures were perfused with
521 extracellular fluid (ECF) containing (in mM): 167 NaCl, 2.4 KCl, 10 glucose, 10 HEPES, 2 $CaCl_2$
522 and 1 $MgCl_2$; NaOH (1 mM) was used to adjust the pH to 7.30, and the osmolarity was adjusted
523 to 305 – 310 mOsm. Tetrodotoxin (TTX) (500 nM) and picrotoxin (PTX) (50 mM) were added to
524 this ECF to block sodium channel-mediated action potentials and $GABA_A$ receptor-mediated
525 currents respectively. Neurons were patched with borosilicate glass pipettes pulled to a tip
526 resistance of 3-6 MΩ when back-filled with intracellular solution containing in (mM): 130 Cs-
527 methanesulfonate, 5 CsCl, 4 NaCl, 1 MgCl, 10 HEPES, 5 EGTA, 5 QX-314 Cl, 0.5 Na-GTP, 10
528 Na-phosphocreatine, and 5 Mg-ATP (~286 mOsm). During experiments, neurons were held at –

529 70 mV in voltage-clamp, with hyperpolarizing voltage steps (-10 mV) performed periodically to
530 measure intrinsic membrane properties. Under these conditions AMPA receptor-mediated
531 miniature excitatory postsynaptic currents (mEPSC)s appeared as transient inward current
532 deflections. Recordings with a series resistance greater than 25 MΩ were excluded from analysis;
533 typical values were between 15 – 20 MΩ. A minimum of 2 minutes following establishment of the
534 whole cell configuration was allowed before experimental measurements, so neurons could fully
535 dialyze with intracellular solution and achieve a stable membrane resistance and holding current.
536 For experiments involving within-cell drug applications, a maximum 20 % change in series
537 resistance between control and drug measurements was tolerated. In these cases, drugs were
538 applied locally to the neuron with a fast perfusion system. Mini Analysis software (Synaptosoft)
539 was used to detect mEPSCs and extract relevant parameters. A minimum of 100 and no more than
540 1000 mEPSC's were analyzed per neuron per experimental condition.
541
542 **Cortical pyramidal neuron morphology:**

543 Cortical pyramidal neurons (CPN)s in WT and YAC128 cultures were labeled by transfecting a
544 subset of neurons (1 of 2.7 million) with a cytoplasmic green fluorescent protein (GFP)
545 (Addgene plasmid 37825) at the time of platting. Cultures were subsequently fixed at DIV17 - 19
546 and GFP-labeled CPN dendritic arbors imaged on a Zeiss Axiovert 200 M fluorescence
547 microscope (20 x magnification, 0.8 NA), with a Zeiss 702 monochrome camera, using Zen
548 software. Multiple image Z-stacks were acquired and X,Y-tiling was used to ensure entire dendritic
549 arbors were visualized. Images were exported to Fiji-ImageJ for analysis by a blinded observer.
550 Images were flattened using the maximum Z-projection function. Background subtraction was

551 performed, and neuronal processes were thresholded following adjustment of brightness and
552 contrast. Automated Sholl analysis was performed using the ImageJ sholl analysis plugin.
553
554 **Excitatory cortical synapse staining:**
555
556 A subset of neurons (2 of 2.7 million) in WT and YAC128 cortical cultures were transfected with
557 a GFP-tagged internally-expressed anti-PSD95 antibody (intrabody) (Gross et al., 2013) at the time
558 of platting. At DIV17 – 19, cells were fixed and stained for VGlut1 and the GluA2 AMPA receptor
559 subunit as previously described (Buren et al., 2016). Briefly, cultures were first live-stained with
560 a primary mouse anti-GluA2 antibody (Millipore), then fixed and stained with a secondary Alexa
561 Fluor 568-conjugated donkey anti-mouse antibody (Invitrogen). Subsequently, cultures were
562 incubated with a primary guinea pig anti-VGlut1 antibody (Millipore), then stained with a
563 secondary AMCA-conjugated donkey anti-guinea pig antibody (Jackson Immuno Research
564 Laboratories). To amplify the GFP fluorescence of the anti-PSD95 intrabody, cultures were also
565 incubated with a primary chicken anti-GFP antibody (1:1000) (Millipore), followed by an
566 secondary Alexa Fluor 488-conjugated antibody (1:500) (Invitrogen). Cultures were imaged on a
567 Zeiss Axiovert 200 M fluorescence microscope (63 x magnification, 1.4 NA), using a Zeiss 702
568 monochrome camera and Zen software. CPNs expressing the anti-PSD95 intrabody were
569 identified based on their diffuse cytoplasmic GFP fill, with bright GFP-labelled puncta expressed
570 at dendritic spines. A portion of each CPNs arbor, containing multiple secondary and tertiary
571 dendrites, was selected for imaging and sufficient image Z-stacks were acquired to adequately
572 capture all dendritic processes present in a given 63x field. Images were exported to Fiji-ImageJ
573 for analysis by a blinded observer and flattened using the maximum Z-projection function. For

574 each CPN image, the GFP channel was used to identify 3 secondary or tertiary dendritic segments,
575 at least 40 µm away from the CPN soma, over which ROIs were drawn. Following background
576 subtraction, fluorescent puncta in the green (GFP), red (Alexa Fluor 568) and blue (AMCA)
577 channels, visible within dendritic ROIs, were manually thresholded and detected with the analyze
578 particles function. The ImageJ colocalization plugin was used to identify triple-colocalized puncta
579 (PSD95, GluA2 and VGlut1), which we interpreted as functional CPN glutamatergic synapses.
580 Synapse density was defined as the number of triple-colocalized puncta present within a dendritic
581 segment divided by the area of the segment and averaged across all 3 dendrites analyzed in a given
582 CPN.
583
584 **Synaptophysin-GCaMP imaging:**
585
586 To directly image cytosolic Ca^{2+} in axonal boutons of neurons in our cortical mono cultures we
587 transfected 1 million cells (of a total 2.7 million) at time of plating with a rat synaptophysin-tagged
588 GCaMP6-M construct (rSyph-GCaMP6m). The rSyph-GCaMP6m construct was created by fusing
589 GCaMP6-M (Chen et al., 2013) with the full length rat synaptophysin protein (1 – 307 amino
590 acids) via a small glycine-serine linker and inserting the fused rSyph-GCaMP6-M construct into a
591 pLL3.7-hSyn vector to achieve neuron-selective expression. For some experiments, the same 1
592 million cells were also transfected at time of platting with an M-cherry-tagged PSD95 construct;
593 in these cases, rSyt-GCaMP6m-expressing presynaptic boutons that colocalized with M-Cherry
594 labeled postsynaptic spines were presumed to be functional synapses.
595

596 For all Ca^{2+}-imaging experiments, cultures were plated on 8-well cover-glass chambers (Thermo
597 Scientific ™, Nunc ™, Lab-Tek ™) and imaged at DIV (17 - 19) with a Zeiss Axiovert 200 M
598 fluorescence microscope (63 x magnification, 1.4 NA), using a Zeiss 702 monochrome camera
599 and Zen software. Movies were acquired at 10 Hz (100 ms exposure per frame) using the Zen
600 time-series mode with camera-steaming enabled. These experiments were performed in standard
601 ECF (as above) with or without TTX (500 nM) present, but in the absence of PTX.
602
603 Spontaneous Ca^{2+} waves were commonly observed in rSyph-GCaMP6m-labelled axons, evident
604 particularly when action potential-dependent Ca^{2+} events were blocked with TTX. Automatically
605 detecting such Ca^{2+} waves proved difficult with algorithms commonly used to quantify activity-
606 related neuronal GCaMP signals. We therefore used the Astrocyte Quantitative Analysis (AQuA)
607 software (running in MATLAB) (Y. Wang et al., 2019) to quantify these waves in the presence of
608 TTX. AQua does not rely on spatially segmenting a Ca^{2+} movie into ROIs based on neuronal
609 morphology, but rather defines events as spatially and temporally connected Ca^{2+} signals
610 surpassing user-defined thresholds. This means spontaneous axonal waves spreading across
611 multiple boutons are typically classified as a single event, because such Ca^{2+}-activity is grouped
612 in time and space. Conversely, a given bouton can be involved in multiple axonal waves and thus
613 detected as part of multiple events, as long as the pertinent signals are sufficiently temporally
614 separated. To compare the frequency of aQua-detected spontaneous axonal events between
615 genotypes and under pharmacological manipulations, we counted numbers of events occurring
616 within a standardized area [178.6 μm x 113.1 μm (a maximal 63 x field of view)], during a
617 standardized (3 min) consecutive imaging interval. The same aQua detection parameters,

618 empirically determined to best match a small number of manually analyzed experiments, were
619 applied across all cultures and conditions analyzed to facilitate meaningful comparisons.
620
621 In a subset of experiments conducted in the presence of TTX, responses of individual WT or
622 YAC128 rSyph-GCaMP6m-labelled synaptic boutons to caffeine or ionomycin were measured. In
623 these experiments culture fields were imaged for 3 min (as above), after which caffeine (1 mM) or
624 ionomycin (10 μM) was applied and imaging continued for an additional 1-2 min. aQua was not
625 used to analyze these experiments, as an ROI-based algorithm was desired. For caffeine
626 applications, an analyzer (blinded to culture genotype) used Fiji-ImageJ (NIH) to manually assign
627 elliptical ROIs to 10 boutons per movie and exported each ROI's fluorescence-intensity time-
628 course. Time-courses were subsequently imported to MATLAB, where the curve fitting tool was
629 used to model each time-course's photobleaching profile based on the initial 3 min recording; this
630 curve was then extrapolated to the entire time-course including caffeine treatment. The resultant
631 "bleaching curve" was subtracted from the raw rSyph-GCaMP6m fluorescence curve and this
632 time-course subsequently divided by the "bleaching curve" to yield a final curve reflecting the
633 caffeine response in DF/F units. Ionomycin experiments were analyzed similarly, except in this
634 case, the blinded analyzer selected 10 active-boutons (showing at least 1 clear Ca^{2+} event during
635 the initial 3 min recording) and 10 inactive-boutons (with no Ca^{2+} events present during the initial
636 3 min recording). Time-courses derived from inactive-boutons were exported to MATLAB, where
637 the ionomycin-mediated DF/F responses were calculated as above. In the case of active-boutons,
638 spontaneous events occurring during the first 3 min were detected with MATLAB's findpeaks
639 function and excised from the raw fluorescence time-courses before curve fitting, but otherwise
640 processed as above.

641

642 As expected, spontaneous events were far more frequent when rSyph-GCaMP6m -expressing
643 cultures where imaged in the absence of TTX. Most boutons showed many events during a 3 min
644 imagining session. These events, which were presumably driven by the action potential-dependent
645 opening of voltage-gated Ca^{2+} channels, were far shorter in duration than typical TTX-resistant
646 events. To assess for genotype differences in these signals, a blinded analyzer used Fiji-ImageJ to
647 randomly assign elliptical ROIs to 20 boutons per movie and exported each ROI's fluorescence-
648 intensity time-course to MATLAB. The high frequency of action potential-dependent events often
649 precluded extracting the photobleaching profile of a bouton's time-course, necessitating an
650 alternative means of calculating the DF/F values of spontaneous events. We therefore averaged
651 the grey-value fluorescence intensity across an entire-time course, subtracted this average
652 fluorescence pointwise from the time-course, then divided pointwise by the average fluorescence
653 to convert to DF/F units. Any nonstationary present in these DF/F time-series due to
654 photobleaching was removed with the MATLAB detrend function. The MATLAB findpeaks
655 function was subsequently used to detect events in these DF/F traces and extract relevant
656 parameters including peak event DF/F amplitudes and event half-amplitude widths. Bouton event
657 frequencies were calculated by dividing numbers of detected events in a DF/F trace by the imaging
658 interval. Bouton event frequencies and event parameters in the absence of TTX were compared
659 between WT and YAC128 cultures under baseline conditions and following application of
660 ryanodine (5 μM).

661

662

663

664 **iGluSnFR imaging in acute brain slices:**

665

666 Expression of the genetically-encoded intensity-based glutamate-sensing fluorescence reporter
667 (iGluSnFR) (Marvin et al. 2013) in WT and YAC128 mice was achieved with stereotaxic injection
668 of a viral construct as described previously (Parsons et al., 2016). Briefly, under isoflurane
669 anesthesia, 1 – 1.4 μl of the AAV1.hSyn.iGluSnFr.WPRE.SV40 construct (Penn Vector Core; Dr.
670 Loren Looger, Janelia Farm Research Campus of the Howard Hughes Medical Institute) was
671 directly injected into the dorsal striatum of 4 – 6 week old mice. Following surgery, mice were
672 closely monitored for a week to ensure adequate recovery.

673

674 After waiting 3 – 6 weeks, to ensure optimal iGluSnFR expression, acute brain slices from 2-3
675 month-old YAC128 mice and age-matched WT controls were prepared as described previously
676 (Parsons et al., 2016; Koch et al., 2018). Briefly, mice were decapitated following deep
677 isoflurane anesthesia and their brains rapidly removed and placed in an ice-cold slicing solution,
678 bubbled with carbogen (95% O_2, 5% CO_2) gas, containing (in mM): 125 NaCl, 2.5 KCl, 25
679 $NaHCO_3$, 1.25 NaH_2PO_4, 2.5 $MgCl_2$, 0.5 $CaCl_2$, and 10 glucose. 300 μm thick striatum-containing
680 sagittal brain slices were cut with a Leica VT1200S vibratome. Slices were subsequently incubated
681 for 30 min in warmed artificial cerebral spinal fluid ACSF containing 2 mM $CaCl_2$ and 1 mM
682 $MgCl_2$; ACSF constituents and concentrations were otherwise identical to the slicing solution
683 (above).

684

685 Slices were transferred to a submerged recording chamber for experiments and perfused with
686 carbogen-bubbled ACSF at a rate of 2 – 3 ml/min at room temperature. Cortical release of

687 glutamate into the striatum was evoked by delivering paired 0.1 ms electrical pulses at 100 Hz
688 with an A-M Systems isolated pulse stimulator (Model 2100) and tungsten monopolar stimulating
689 electrode (tip resistance - 0.1 MΩ). The electrode was placed into a corpus callosum segment
690 adjacent to the dorsal striatum at an approximate 50 – 100 μm depth. During and immediately prior
691 to the electrical stimulation, iGluSnFR fluorescence was excited with a 470 nm LED; slices were
692 not illuminated between experimental measurements to minimize phototoxicity and bleaching.
693 Stimulation and LED activation were triggered by Clampex software (Molecular Devices,
694 Sunnyvale, CA). iGluSnFR fluorescence was isolated with a 530 nm bandpass filter and imaged
695 with a CCD camera (1 M60, Pantera, Dalsa) and XCAP software (Epix, inc.) at 150 Hz with 8 x
696 8-pixel binning. Experimental measurements encompassing four stimulation trials and two blank
697 trial were performed at 3-minute intervals. The four stimulation trials were averaged and the blank
698 trials, in which slice-fluorescence was imaged without electrical stimulation, were averaged and
699 used to account for photobleaching and to calculate the stimulation mediated changes in iGluSnFR
700 fluorescence over basal fluorescence (ΔF/F) as described previously (Parsons et al., 2016).
701 Videos were analyzed offline with ImageJ software. The average iGluSnFR signal was measured
702 over 10 x 10-pixel (93.8 x 93.8 μM) region of interested (ROI) placed over the maximal area of
703 evoked iGSnFR activity within the striatum adjacent to the stimulating electrode.
704
705 **Experimental design and statistical analysis:**
706
707 Statistical analysis and creation of figures was performed using GraphPad Prism (version 7). All
708 data distributions were tested for normality with the D'Agostino-Pearson omibus normality test.
709

710 The Student's unpaired t-test was used for unpaired comparisons between two data groups, such
711 as when mean mEPSC frequencies were compared between WT and YAC128 neurons, as long
712 both data groups were normally distributed. When one or both groups failed the D'Agostino-
713 Pearson omibus normality test, the non-parametric Mann Whitney test was used instead.
714
715 When parameters of the same group of neurons or axonal boutons were compared before and after
716 a drug treatment, statistical significance was assessed with the Student's paired t-test, unless data
717 points in the control or drug-treatment group failed the D'Agostino-Pearson omibus normality test;
718 in which case, the non-parametric Wilcoxon matched-pairs signed rank test was used instead.
719
720 A two-way ANOVA with the Bonferroni post-test was used when testing for genotype differences
721 in a dependent variable measured at different time points, as was the case for our brain-slice
722 iGluSnFR experiments.
723
724 Depending on the experimental design, "n" numbers in figures refer either to number of neurons,
725 numbers of imaged culture fields, numbers of individual axonal boutons, or numbers of brain
726 slices. Clarifying details are present within individual figure legends, as are the numbers of culture
727 batches or mice used.
728
729 Differences in mean values were considered significant at $p<0.05$, and significance levels are
730 indicated in figures as follows: *$p<0.05$, **$p<0.01$, ***$p<0.001$, ***$p<0.0001$. Comprehensive
731 descriptions of statistical analysis are included in figure legends.
732

Acknowledgments

We thank Dr. Anne Marie Craig (UBC) for expert advice on experiments using rSyph-GCaMP6m, and Dr. Lily Zhang and Dr. Rujun Kang for technical support and assistance. The work was supported by funding from the Canadian Institutes of Health Research (CIHR) Foundation grants FDN-143210 to LAR and FDN-154278 to MRH. CB was supported by a University of British Columbia 4-year Graduate Fellowship (UBC 4-YF). ASD was supported by a CIHR Canada Graduate Scholarship Doctoral award and a UBC 4-YF. EK was supported by a CIHR Canada Graduate Scholarship Master's award and UBC 4-YF. MES was supported by a Vanier Canada Graduate Scholarship and a UBC 4-YF. WN was supported by a UBC-CIHR-MD/PhD studentship and a Vanier Canada Graduate Scholarship. LAR holds the UBC Department of Psychiatry Louise A. Brown Chair in Neuroscience. MRH holds a Canada Research Chair.

Declaration of Interests

The authors declare no competing interests.

756 **Figure legends:**

757

758 **Fig 1: YAC128 cortical cultures show elevated miniature EPSC frequencies at early DIV**
759 **time points.**

760 Representative traces (**A, D, G, J**) and population data for mEPSCs (frequency in **B, E, H, K**;
761 amplitude in **C, F, I, L**) recorded from WT and YAC128 CPNs. All recordings were made in
762 voltage clamp with a holding potential of -70mV in solution containing TTX (500 nM) and PTX
763 (50 μM).

764 **A – C:** Recordings made from CPNs in DIV-7 cultures**.** Mean mEPSC frequency (**B**) was 1.8 ±
765 0.3 Hz (n=18; 3 cultures) in WT CPNs and 2.8 ± 0.7 Hz (n=17; 4 cultures) in YAC CPNs; this
766 difference was not statistically significantly [t(33)=1.449; p=0.1567; Student's unpaired-t test].
767 Mean mEPSC amplitudes (**C**) were similar in WT and YAC128 cultures: 17.2 ± 1.5 pA (n=18; 3
768 cultures) and 17.0 ± 1.7 pA (n=17; 4 cultures) respectively [t(33)=0.06936; p=0.9452; Student's
769 unpaired-t test].

770 **D - F:** Recordings were made from CPNs in DIV-14 cortical cultures. Mean mEPSC frequency
771 (**E)** was significantly higher in YAC128 CPNs [10.8 ± 1.8 Hz (n=20; 6 cultures)] compared to WT
772 CPNs [4.4 ± 2.6 Hz (n=22; 4 cultures)], [t(40)=3.555; p=0.0010; Student's unpaired-t test]. Mean
773 CPN mEPSC amplitudes (**F**) were not significantly different in WT and YAC128 cultures: 12.1 ±
774 0.8 pA (n=22; 4 cultures) and 15.0 ± 1.4 pA (n=20; 6 cultures), respectively [t(40)=1.807;
775 p=0.0786; Student's unpaired-t test].

776 **G – I:** Recordings were made from CPNs in DIV-18 cortical cultures. Mean CPN mEPSC
777 frequency (**H**) was significantly higher in YAC128 cortical cultures [14.1 ± 1.2 Hz (n=38; 10
778 cultures)] compared to WT cultures [9.9 ± 1.5 Hz (n=30; 15 cultures)], [p<0.0059 (exact); Mann

779 Whitney test]. Mean CPN mEPSC amplitudes (**I**) were similar in WT and YAC128 cultures: 17.0
780 ± 1.8 pA (n=30; 15 cultures) and 17.4 ± 1.8 pA (n=38; 10 cultures) respectively [p=0.8643 (exact);
781 Mann Whitney test].
782 **J – L:** Recordings were made from CPNs in DIV-21 cortical cultures. Mean CPN mEPSC
783 frequency (**K**) was similar in WT and YAC128 cultures: 14.2 ± 1.2 Hz (n=62; 17 cultures) and
784 14.0 ± 0.9 Hz (n=71, 23 cultures), respectively [p=0.5626 (exact); Mann Whitney test]. Mean CPN
785 mEPSC amplitudes (**L**) were similar in WT and YAC128 cultures: 22.3 ± 1.3 pA (n=62; 17
786 cultures) and 24.3 ± 1.2 pA (n=71; 23 cultures), respectively [p=0.2143 (exact); Mann Whitney
787 test].
788
789 **Supplemental Fig 1: Dendritic complexity and excitatory synapse numbers are similar in**
790 **WT and YAC128 cortical cultures.**
791 **A, B.** Representative images generated by thresholding a merged Z-stack of a green fluorescent
792 protein (GFP)-expressing WT CPN (**A**) and YAC128 CPN (**B**).
793 **C.** Number of dendritic intersections through concentric sholl circles centered on the soma of GFP-
794 filled WT and YAC128 CPNs of radii between 10 μm and 450 μm. WT and YAC128 CPNs have
795 nearly identical dendritic branching distributions [2-way ANOVA; Genotype: F(1, 6165)= 1.168,
796 p<0.2799; Distance from soma: F(44, 6165)=381.6, p<0.0001; Interaction: F(44, 6165)=0.9868,
797 p<0.4966].
798 **D.** Total numbers of sholl intersections, which reflect general neuronal complexity, were similar
799 in WT and YAC128 CPNs: 254.0 ± 8.8 (n=61; 4 cultures) and 249.5 ± 8.7 (n=78; 4 cultures)
800 respectively [p=0.7263 (exact); Mann Whitney test].

801 **E.** A representative merged Z-stack from a WT CPN (left panels) and YAC128 CPN (right panels)
802 with merged green, red and blue channels showing staining of a genetically-encoded internally-
803 expressed GFP-tagged anti-PSD-95 antibody (green), anti AMPA receptor GluA2 subunit
804 immuno-staining (red) and anti VGlut1 immuno-staining (blue) respectively. The bottom panel
805 shows an expanded view of a segment of dendrite with arrows pointing to a subset of co-localized
806 PSD-95, GluA2 and VGlut1 puncta, which were counted as presumed functional synapses. Note,
807 for illustrative purposes the brightness and contrast of the individual channels were adjusted to
808 best illustrate the punctate fluorescence.
809 **F**. Numbers of presumed functional synapses (identified as above) per 100 μm^2 of secondary and
810 tertiary dendrites of WT and YAC128 CPNs: 8.8 ± 1.1 (n=37; 2 cultures) and 6.8 ± 0.7 (n=57; 3
811 cultures), respectively. Although synapse numbers were lower in YAC128 cultures this did not
812 reach statistical significance [p=0.1039 (exact); Mann Whitney test].
813
814 **Fig 2: Spontaneous release of ER Ca^{2+} elevates YAC128 pyramidal neuron miniature EPSC**
815 **frequencies.**
816 **A and B - Hypothetical model (tested below) A.** We hypothesize, in WT cultures, spontaneous
817 Ca^{2+} release from ER stores in presynaptic cortical terminals only minimally augments action
818 potential-independent (mini) glutamate release. **B.** Conversely, in YAC128 cultures, we
819 hypothesize spontaneous Ca^{2+} release from presynaptic ER stores is increased, and that this
820 elevates Ca^{2+}-dependent, mini glutamate release.
821 **C – H:** Voltage clamp recordings were made at -70 mV from DIV-18 cultured WT (**C – E**) and
822 YAC128 CPNs (**F – H**) in the presence of TTX (500 nM) and PTX (50 μM), under control
823 conditions and during subsequent local ryanodine (5 μM) application. Note that in the

824 representative traces from the WT CPN (**C**), ryanodine (5 μM) substantially increased the mEPSC
825 frequency, whereas the drug had little effect on the mEPSC frequency in the representative
826 YAC128 CPN (**F**). Quantifying the population data revealed that ryanodine (5 μM) significantly
827 increased the mean mEPSC frequency in WT cultured CPNs (**D**) from 6.7 ± 1.2 Hz to 11.9 ± 2.4
828 Hz, [t(12)=2.50; p=0.0280; n=13; 8 cultures; Student's paired-t test]. Ryanodine (5 μM) did not
829 significantly affect the mean WT CPN mEPSC amplitude (**E**) (control: 21.0 ± 3.2 pA, ryanodine:
830 20.2 ± 2.3 pA), [t(12)=0.65; p=0.5278; n=13; 8 cultures; Student's paired-t test]. In YAC128
831 cultures, ryanodine (5 μM) did not significantly affect the mean CPN mEPSC frequency (**G**)
832 (control: 12.0 ± 1.7 Hz, ryanodine: 13.9 ± 2.0 Hz), [t(14)=1.65; p=0.1206; n=15; 4 cultures;
833 Student's paired-t test]. Ryanodine (5 μM) also did not significantly affect the mean CPN mEPSC
834 amplitude (**H**) (control: 20.5 ± 4.4 pA, ryanodine: 19.6 ± 3.4 pA), [t(14)=0.71; p=0.4904; n=15; 4
835 cultures; Student's paired-t test].
836 **I.** Voltage clamp recordings from representative WT (top) and YAC128 (bottom) CPNs at -70 mV
837 in the presence of TTX (500 nM) and PTX (50 μM) (as before), with the addition of CPA (30 μM)
838 and in the absence of extracellular Ca^{2+}. Note in all such recording, CPNs were incubated in this
839 CPA-containing, 0 mM Ca^{2+} ECSF for a minimum of 10 min.
840 **J.** In CPA (30 μM) and in the absence of extracellular Ca^{2+}, mEPSCs were significantly less
841 frequent in YAC128 CPNs [3.3 ± 0.6 Hz (n=14; 4 cultures)] compared WT CPNs [8.4 ± 1.5 Hz
842 (n=17; 5 cultures)] under like conditions [t(29)=2.952; p=0.0062; Student's unpaired-t test].
843 **K.** In CPA (30 μM) and in the absence of extracellular Ca^{2+}, YAC128 CPNs showed a trend
844 towards a lower mean mEPSC amplitude than in WT (WT: 26.7 ± 5.2 pA, YAC128: 16.1 ± 3.3

845 pA), but this did not reach statistical significance [t(27)=1.706; p=0.0995; Student's unpaired-t
846 test].
847
848
849 **Supplemental Fig 2: Releasing ER Ca^{2+} with caffeine increases the CPN mEPSC frequency**
850 **in WT, but not YAC128, CPNs.**
851 Voltage clamp recordings were made from cultured WT and YAC128 CPNs at -70 mV in the
852 presence of TTX (500 nM) and PTX (50 μM), under control conditions and during subsequent
853 local caffeine (1 mM) application.
854 **A, D:** Representative traces from WT (A) and YAC128 (D) CPNs, under control (top traces) and
855 caffeine (bottom traces) conditions. In this CPN, caffeine (1 mM) substantially increased the
856 mEPSC frequency.
857 **B.** Caffeine (1 mM) significantly increased the mean mEPSC frequency in WT cultured CPNs
858 from 12.3 ± 2.5 Hz to 22.8 ± 8.0 Hz, [p=0.0076 (exact); n=16; 8 cultures; Wilcoxon matched-pairs
859 signed rank test].
860 **C.** Caffeine (1 mM) did not significantly affect the mean WT CPN mEPSC amplitude (control:
861 13.7 ± 1.9 pA, caffeine: 17.2 ± 3.4 pA), [p=0.8603 (exact); n=16; 8 cultures; Wilcoxon matched-
862 pairs signed rank test].
863 **E.** In YAC128 CPNs, caffeine (1 mM) did not significantly affect the mean CPN mEPSC
864 frequency (control: 12.0 ± 2.1 Hz, caffeine: 11.5 ± 1.9 Hz), [t(12)=0.4808; p=0.6393; n=13; 5
865 cultures; Student's paired-t test].

866 **F.** In YAC128 CPNs, caffeine (1 mM) also did not significantly affect the mean CPN mEPSC
867 amplitude (control: 14.5 ± 1.4 pA, caffeine: 14.1 ± 1.2 pA), [t(12)=0.8086; p=0.4345; n=13; 5
868 cultures; Student's paired-t test].
869 **G.** Percent change in mEPSC frequency mediated by Caffeine (1 mM) application to WT and
870 YAC128 CPNs (calculated from the responses in panels **B** and **E**). Caffeine (1 mM) elicited a
871 significantly greater increase in the mEPSC frequency in WT, compared to YAC128, CPNs [WT:
872 99.2 ± 34.1 % (n=16; 8 cultures), YAC128: 1.2 ± 7.6 % (n=13; 5 cultures)], [p=0.0025 (exact);
873 Mann Whitney test].
874
875
876 **Fig 3: Axonal Ca^{2+} waves are more frequent in YAC128 Cortical Cultures.**
877 **A.** Portion of a YAC128 rat synaptophysin-tagged GCaMP6-M (rSyph-GCaMP6m)-expressing
878 axon during a spontaneous Ca^{2+} wave in the presence of ECF containing TTX (500 nM). Images
879 reflect raw GCaMP fluorescence values (arbitrary units) and comprise 15 s of a 4 min video. For
880 illustrative purposes, images were binned temporally from the original 10 Hz movie, such that
881 each 2 s frame reflects the average fluorescence of 20 successively acquired frames.
882 **B.** Time course of DF/F (change in fluorescence over basal fluorescence) values extracted from 3
883 of the YAC128 rSyph-GCaMP6m-expressing axonal boutons (shown in panel **A** with color-coded
884 arrows, panel labelled 15s). Signals were spatially averaged across elliptical regions of interest
885 (ROI)s encompassing the indicated boutons and represent the entire 4 min imaging session. Note
886 the multi-second delay in the propagation of signals between boutons and the long time course of
887 individual events.

888 **C.** Representative 3 min DF/F time course from a WT rSyph-GCaMP6m-expressing axonal bouton
889 in TTX (500 nM) (top). Note the substantially longer duration of this event compared to
890 representative events recorded without TTX from a separate WT rSyph-GCaMP6m-expressing
891 bouton (bottom).
892 **D.** Average half amplitude width of spontaneous Ca^{2+} events occurring in rSyph-GCaMP6m-
893 expressing boutons in WT and YAC128 cortical cultures in the presence and absence of TTX (500
894 nM). Select comparisons were made with the Mann Whitney test because event widths in all
895 groups failed the D'Agostino-Pearson omibus normality test. WT events were significantly longer
896 with TTX [8.60 ± 0.92 s (n=164 events; 85 boutons; 4 cultures)] than without [1.06 ± 0.97 s
897 (n=3725 events; 175 boutons; 4 cultures)] [p<0.0001 (approximate); Mann Whitney test].
898 Likewise, YAC128 half widths were significantly longer with TTX [6.23 ± 0.35 s (n=440 events;
899 153 boutons; 4 cultures)] than without [1.17 ± 1.46 s (n=5159 events; 422 boutons; 6 cultures)]
900 [p<0.0001 (approximate); Mann Whitney test].
901 **E.** Numbers of detected spontaneous axonal events (as in Panels **A** and **B**) during 3 min recordings
902 of 63 x objective (178.6 μm x 113.1 μm) fields imaged in the presence of TTX (500 nM). Action
903 potential-independent events were significantly more frequent in YAC128 cortical cultures [115.9
904 ± 28.1 events/3 min (n=15 fields; 4 cultures)], compared to WT [36.3 ± 5.5 events/3 min (n=12
905 fields; 4 cultures)], [p=0.0016 (exact); Mann Whitney test].
906 **F.** Average peak DF/F amplitudes of all the spontaneous, action potential-independent axonal Ca^{2+}
907 events imaged in a given 63 x objective field over 3 min from WT and YAC128 cortical cultures.
908 Average event amplitudes were not significantly different between WT [0.240 ± 0.046 DF/F (n=10
909 fields; 4 cultures)] and YAC128 cultures [0.216 ± 0.027 DF/F (n=12 fields; 4 cultures)],
910 [t(20)=0.465; p=0.647; Student's unpaired-t test].

911

912 **Fig 4: Boutons spontaneously active in TTX show relatively elevated cytosolic Ca^{2+} in both**
913 **genotypes. Resting cytosolic Ca^{2+} concentrations are higher in the overall YAC128 bouton**
914 **population.**

915 **A.** DF/F time courses from two rSyph-GCaMP6m-expressing axonal boutons from a
916 representative YAC128 culture in the presence of TTX (500 nM). The first bouton (top trace) is
917 inactive during the 3 min imaging session, while the second bouton (bottom trace) shows a clear
918 spontaneous event (black arrow). Subsequent application of the Ca^{2+} ionophore ionomycin (10
919 μM) elicits a smaller Ca^{2+} response in the spontaneously active bouton, suggesting a higher basal
920 cytosolic Ca^{2+} concentration (pre-ionomycin) in the active bouton.

921 **B,C:** Ionomycin responses of rSyph-GCaMP6m-expressing boutons in the presence of TTX
922 following a 3 min imaging session in WT (**B**) and YAC128 (**C**) cultures. Boutons were classified
923 as active or inactive based on the presence, or lack thereof, of at least one spontaneous Ca^{2+} event
924 during the initial 3 minute recording. Ionomycin responses were significantly larger in the
925 population of inactive boutons [WT: 0.633 ± 0.072 DF/F (n=67 boutons); YAC128: 0.410 ± 0.040
926 DF/F (n=51 boutons)], vs active boutons [WT: 0.191 ± 0.026 DF/F (n=41 boutons; 4 cultures),
927 $p<0.0001$ (exact) by Mann Whitney test; YAC128: 0.149 ± 0.016 DF/F (n=46 boutons), $p<0.0001$
928 (exact) by Mann Whitney test]. 4 cultures for WT and 4 cultures for YAC128.

929 **D, E:** Responses of rSyph-GCaMP6m-expressing axons from a representative WT (**D**) and
930 YAC128 (**E**) cortical culture to ionomycin (10 μM). Images are from a 4 min imaging session,
931 with ionomycin application at 3 min and reflect raw GCaMP fluorescence values (arbitrary units)
932 (as above). To minimize impacts of photobleaching, the top (before) image is the frame
933 immediately prior ionomycin. The bottom image is a maximum projection of all frames acquired

934 30s prior and following ionomycin treatment and reflect each pixel's maximum ionomycin
935 response. The visible grey-value dynamic range is the same in panels **D** and **E**, (150 increments of
936 the total unprocessed 14 bit-depth), however the 0 value in **E** has been adjusted so that brightness
937 of the before image is comparable to that of its WT counterpart in **D**; this is so the reader can better
938 appreciate the YAC128 culture's smaller relative change in fluorescence.
939 **F.** Ionomycin responses of the all WT and YAC128 rSyph-GCaMP6m-expressing axons
940 automatically detected with the aQua software suite (see methods for reference). The WT bouton
941 population showed a significantly greater ionomycin-mediated change in fluorescence [0.272 ±
942 0.006 DF/F (n=1681 boutons; 4 cultures)] compared to the YAC128 population [0.190 ± 0.002
943 DF/F (n=1462 boutons; 4 cultures)], [p<0.0001 (exact); Mann Whitney test].
944
945 **Fig 5: Caffeine increases the frequency of spontaneous Ca^{2+} events and the resting Ca^{2+}**
946 **concentration in WT, but not YAC128, cortical axonal boutons.**
947 **A, B:** Numbers of detected spontaneous rSyph-GCaMP6m axonal events in the presence TTX
948 (500 nM) during 3 min recordings of 63 x objective fields of WT (**A**) and YAC128 (**B**) cortical
949 cultures (as above). The control group consists of the same culture fields shown in **Figure 6: E**,
950 and is compared to separate WT (**A**) or YAC128 (**B**) culture fields imaged in the presence of
951 caffeine (1 mM) under otherwise like conditions. WT axons showed significantly more action
952 potential-independent events in the presence of caffeine, than in its absence [203.8 ± 55.2 events/3
953 min (n=10 fields; 5 cultures)] vs [36.3 ± 5.5 events/3 min (n=12 fields; 4 cultures)] respectively
954 [t(20)=3.316; p=0.0034; Student's unpaired-t test]. Numbers of detected YAC128 axonal events
955 were not significantly different in the presence or absence of caffeine [115.1 ± 28.21 events/3 min

956 (n=15 fields; 4 cultures)] vs [150.0 ± 28.55 events/3 min (n=8 fields; 4 cultures)] respectively
957 [p=0.2188 (exact); Mann Whitney test].
958 **C.** DF/F time courses from representative WT (top) and YAC128 (bottom) rSyph-GCaMP6m-
959 expressing axonal boutons in the presence of TTX (500 nM) before and immediately following
960 application of caffeine (1 mM). For this illustration, boutons were selected which did not show
961 spontaneous events. Rather, note the gradual sustained increase in rSyph-GCaMP6m fluorescence,
962 which is of larger magnitude in the WT bouton.
963 **D.** Caffeine responses of WT and YAC128 rSyph-GCaMP6m-expressing boutons in the presence
964 of TTX as illustrated in panel **C.** Boutons showing spontaneous events **(as in Figure 6)** were
965 excluded as the long time course of such events complicated quantification of steady-state
966 increases in DF/F. Caffeine application elicited a significantly greater increase in rSyph-
967 GCaMP6m fluorescence in WT boutons [0.342 ± 0.030 DF/F (n=87 boutons)] compared to
968 YAC128 [0.229 ± 0.039 DF/F (n=54 boutons)] [p=0.0004 (exact); Mann Whitney test]. For A, B
969 and D: 5 cultures for WT and 5 cultures for YAC128.
970
971 **Fig 6: In the absence of TTX, presynaptic calcium events are more frequent in WT,**
972 **compared to YAC128, cultures.**
973 **A, B:** DF/F time course from representative WT rSyph-GCaMP6m-expressing axonal boutons in
974 the absence of TTX, under control conditions (A) and in presences of 5 μM ryanodine (B). Note
975 these are not the same boutons, as experiments illustrated in this figure were not paired.
976 **C, D:** DF/F time course from two different representative YAC128 rSyph-GCaMP6m-expressing
977 axonal boutons in the absence of TTX, one under control conditions (C) and the other in the
978 presence of 5 μM ryanodine. (D)

979 **E:** Mean Ca^{2+} event frequencies of rSyph-GCaMP6m-expressing boutons in the absence of TTX
980 in WT and YAC128 cortical cultures in the presence and absence of ryanodine (5 μM). Select
981 comparisons were made with the Mann Whitney test because event widths in all groups failed the
982 D'Agostino-Pearson omibus normality test. Events were significantly more frequent in WT
983 boutons [0.1424 ± 0.0061 Hz (n=272 boutons; 5 cultures)] than in YAC128 boutons [0.0761 ±
984 0.0044 Hz (n=423 boutons; 6 cultures)] [p<0.0001 (approximate); Mann Whitney test]. Events
985 were significantly less frequent in WT boutons with ryanodine (5 μM) [0.1179 ± 0.0033 Hz (n=120
986 boutons, 3 cultures)] than without (above) [p=0.0038 (approximate); Mann Whitney test].
987 Conversely, event frequencies were significantly more frequent in YAC128 boutons with
988 ryanodine (5 μM) [0.0886 ± 0.0044 Hz (n=189 boutons, 4 cultures)] than without (above)
989 [p=0.0003 (approximate); Mann Whitney test].
990 **F, G:** DF/F time course from two representative rSyph-GCaMP6m-expressing axonal boutons
991 from the same WT culture field in the absence of TTX. Bouton (F) shows only faster events (lasting
992 < 6 s), while in bouton (G) a clear slow event (lasting >6 s) is present. Note the substantially lower
993 overall event frequency in (G).
994 **H, I:** Ca^{2+} event frequencies of WT (H) and YAC128 (I) rSyph-GCaMP6m-expressing boutons
995 (as above), grouped based on the presence or absence of one or more slow events (> 6 s at half
996 peak amp). (H): 23/292 (7.9 %) WT boutons showed at least on such slow event with an overall
997 mean bouton frequency of 0.107 ± 0.016 Hz (n=23), significantly lower than WT boutons lacking
998 slower events [0.143 ± 0.006 Hz (n=269)] [p=0.0058 (exact); Mann Whitney test] (n=292 boutons,
999 5 cultures). (I) 44/423 (10.4 %) YAC128 boutons showed at least one such slow event with an
1000 overall mean bouton frequency of 0.052 ± 0.005 Hz (n=44), significantly lower than YAC128

1001 boutons lacking slower events [0.076 ± 0.004 Hz (n=379)] [p=0.0058 (exact); Mann Whitney test]
1002 (n=423 boutons, 6 cultures).
1003
1004 **Fig 7: Ryanodine reduces evoked striatal iGluSnR responses in WT, but not YAC128, brain**
1005 **slices.**
1006 **A.** Image of raw iGluSnFR fluorescence from a representative WT mouse brain slice with viral-
1007 mediated expression of iGluSnFR in its dorsal striatum. Note the square ROI over which evoked
1008 spatially averaged DF/F signals were measured, and the tungsten monopolar stimulating electrode
1009 placed in the corpus callosum.
1010 **B.** A DF/F image montage from the WT brain slice (shown in A), illustrating a striatum iGluSnFR
1011 response evoked by electrically stimulating cortical axons in the adjacent corpus callosum.
1012 **C.** Striatum evoked DF/F iGluSnFR responses from a representative WT (top) and YAC128
1013 (bottom) brain slice before and in the presence of ryanodine (5 μM). Ryanodine elicits a substantial
1014 reduction in the peak WT, but not YAC128, iGluSnFR response.
1015 **D.** Peak evoked striatum iGluSnFR responses from WT and YAC128 slices before and during
1016 treatment of slices with ryanodine (5 μM). Responses were measured repeatedly at 3 min intervals
1017 and were normalized to the average of each slice's 3 baseline (before drug) measurements.
1018 Ryanodine application decreased the amplitude of the evoked iGluSnFR response in WT (n=9
1019 slices; 9 mice), but not YAC128 (n=8 slices; 8 mice). The effect of ryanodine on WT slices was
1020 significantly different than in YAC128 slices, based on a significant time-genotype interaction
1021 (p=0.0094, repeated measure (time) two way ANOVA).
1022
1023

1024

1025

1026 **References:**
1027

1028 A novel gene containing a trinucleotide repeat that is expanded and unstable on Huntington“s
1029 disease chromosomes. The Huntington”s Disease Collaborative Research Group, 1993. A
1030 novel gene containing a trinucleotide repeat that is expanded and unstable on Huntington“s
1031 disease chromosomes. The Huntington”s Disease Collaborative Research Group. Cell 72,
1032 971–983.
1033 Atasoy, D., Ertunc, M., Moulder, K.L., Blackwell, J., Chung, C., Su, J., Kavalali, E.T., 2008.
1034 Spontaneous and evoked glutamate release activates two populations of NMDA receptors
1035 with limited overlap. J. Neurosci. 28, 10151–10166. doi:10.1523/JNEUROSCI.2432-
1036 08.2008
1037 Bachoud-Lévi, A.-C., Ferreira, J., Massart, R., Youssov, K., Rosser, A., Busse, M., Craufurd, D.,
1038 Reilmann, R., De Michele, G., Rae, D., Squitieri, F., Seppi, K., Perrine, C., Scherer-Gagou,
1039 C., Audrey, O., Verny, C., Burgunder, J.-M., 2019. International Guidelines for the
1040 Treatment of Huntington's Disease. Front Neurol 10, 710. doi:10.3389/fneur.2019.00710
1041 Beal, M.F., Kowall, N.W., Ellison, D.W., Mazurek, M.F., Swartz, K.J., Martin, J.B., 1986.
1042 Replication of the neurochemical characteristics of Huntington's disease by quinolinic acid.
1043 Nature 321, 168–171. doi:10.1038/321168a0
1044 Beaulieu-Laroche, L., Harnett, M.T., 2018. Dendritic Spines Prevent Synaptic Voltage Clamp.
1045 Neuron 97, 75–82.e3. doi:10.1016/j.neuron.2017.11.016
1046 Botelho, E.P., Wang, E., Chen, J.Y., Holley, S., Andre, V., Cepeda, C., Levine, M.S., 2014.
1047 Differential Synaptic and Extrasynaptic Glutamate-Receptor Alterations in Striatal Medium-
1048 Sized Spiny Neurons of Aged YAC128 Huntington's Disease Mice. PLoS Currents 6.
1049 doi:10.1371/currents.hd.34957c4f8bd7cb1f5ec47381dfc811c3
1050 Budde, T., Meuth, S., Pape, H.-C., 2002. Calcium-dependent inactivation of neuronal calcium
1051 channels. Nat. Rev. Neurosci. 3, 873–883. doi:10.1038/nrn959
1052 Buren, C., Parsons, M.P., Smith-Dijak, A., Raymond, L.A., 2016. Impaired development of
1053 cortico-striatal synaptic connectivity in a cell culture model of Huntington's disease.
1054 Neurobiol. Dis. 87, 80–90. doi:10.1016/j.nbd.2015.12.009
1055 Cens, T., Rousset, M., Leyris, J.-P., Fesquet, P., Charnet, P., 2006. Voltage- and calcium-
1056 dependent inactivation in high voltage-gated Ca(2+) channels. Prog. Biophys. Mol. Biol. 90,
1057 104–117. doi:10.1016/j.pbiomolbio.2005.05.013
1058 Cepeda, C., Hurst, R.S., Calvert, C.R., Hernández-Echeagaray, E., Nguyen, O.K., Jocoy, E.,
1059 Christian, L.J., Ariano, M.A., Levine, M.S., 2003. Transient and progressive
1060 electrophysiological alterations in the corticostriatal pathway in a mouse model of
1061 Huntington's disease. J. Neurosci. 23, 961–969.
1062 Chen, T.-W., Wardill, T.J., Sun, Y., Pulver, S.R., Renninger, S.L., Baohan, A., Schreiter, E.R.,
1063 Kerr, R.A., Orger, M.B., Jayaraman, V., Looger, L.L., Svoboda, K., Kim, D.S., 2013.
1064 Ultrasensitive fluorescent proteins for imaging neuronal activity. Nature 499, 295–300.
1065 doi:10.1038/nature12354
1066 de Juan-Sanz, J., Holt, G.T., Schreiter, E.R., de Juan, F., Kim, D.S., Ryan, T.A., 2017. Axonal
1067 Endoplasmic Reticulum Ca 2+ Content Controls Release Probability in CNS Nerve
1068 Terminals. Neuron 93, 867–881.e6. doi:10.1016/j.neuron.2017.01.010
1069 Dunwiddie, T.V., Masino, S.A., 2001. The role and regulation of adenosine in the central
1070 nervous system. Annu. Rev. Neurosci. 24, 31–55. doi:10.1146/annurev.neuro.24.1.31

1071 Emptage, N.J., Reid, C.A., Fine, A., 2001. Calcium Stores in Hippocampal Synaptic Boutons
1072 Mediate Short-Term Plasticity, Store-Operated Ca2+ Entry, and Spontaneous Transmitter
1073 Release. Neuron 29, 197–208. doi:10.1016/S0896-6273(01)00190-8
1074 Espinosa, F., Kavalali, E.T., 2009. NMDA Receptor Activation by Spontaneous Glutamatergic
1075 Neurotransmission. J. Neurophysiol. 101, 2290–2296. doi:10.1152/jn.90754.2008
1076 Fan, M.M.Y., Fernandes, H.B., Zhang, L.Y.J., Hayden, M.R., Raymond, L.A., 2007. Altered
1077 NMDA receptor trafficking in a yeast artificial chromosome transgenic mouse model of
1078 Huntington's disease. J. Neurosci. 27, 3768–3779. doi:10.1523/JNEUROSCI.4356-06.2007
1079 Fishbein, I., Segal, M., 2007. Miniature synaptic currents become neurotoxic to chronically
1080 silenced neurons. Cereb. Cortex 17, 1292–1306. doi:10.1093/cercor/bhl037
1081 Frank, C.A., Kennedy, M.J., Goold, C.P., Marek, K.W., Davis, G.W., 2006. Mechanisms
1082 underlying the rapid induction and sustained expression of synaptic homeostasis. Neuron 52,
1083 663–677. doi:10.1016/j.neuron.2006.09.029
1084 Fredj, N.B., Burrone, J., 2009. A resting pool of vesicles is responsible for spontaneous vesicle
1085 fusion at the synapse. Nat. Neurosci. 12, 751–758. doi:10.1038/nn.2317
1086 Graveland, G.A., Williams, R.S., DiFiglia, M., 1985. Evidence for degenerative and regenerative
1087 changes in neostriatal spiny neurons in Huntington's disease. Science 227, 770–773.
1088 Gross, G.G., Junge, J.A., Mora, R.J., Kwon, H.-B., Olson, C.A., Takahashi, T.T., Liman, E.R.,
1089 Ellis-Davies, G.C.R., McGee, A.W., Sabatini, B.L., Roberts, R.W., Arnold, D.B., 2013.
1090 Recombinant probes for visualizing endogenous synaptic proteins in living neurons. Neuron
1091 78, 971–985. doi:10.1016/j.neuron.2013.04.017
1092 Hantraye, P., Riche, D., Maziere, M., Isacson, O., 1990. A primate model of Huntington's
1093 disease: behavioral and anatomical studies of unilateral excitotoxic lesions of the caudate-
1094 putamen in the baboon. Exp. Neurol. 108, 91–104.
1095 Joshi, P.R., Wu, N.-P., André, V.M., Cummings, D.M., Cepeda, C., Joyce, J.A., Carroll, J.B.,
1096 Leavitt, B.R., Hayden, M.R., Levine, M.S., Bamford, N.S., 2009. Age-dependent alterations
1097 of corticostriatal activity in the YAC128 mouse model of Huntington disease. J. Neurosci.
1098 29, 2414–2427. doi:10.1523/JNEUROSCI.5687-08.2009
1099 Kavalali, E.T., 2015. The mechanisms and functions of spontaneous neurotransmitter release.
1100 Nat. Rev. Neurosci. 16, 5–16. doi:10.1038/nrn3875
1101 Kovalenko, M., Milnerwood, A., Giordano, J., St Claire, J., Guide, J.R., Stromberg, M., Gillis,
1102 T., Sapp, E., DiFiglia, M., MacDonald, M.E., Carroll, J.B., Lee, J.-M., Tappan, S.,
1103 Raymond, L., Wheeler, V.C., 2018. HttQ111/+ Huntington's Disease Knock-in Mice Exhibit
1104 Brain Region-Specific Morphological Changes and Synaptic Dysfunction. J Huntingtons Dis
1105 7, 17–33. doi:10.3233/JHD-170282
1106 Lindhout, F.W., Cao, Y., Kevenaar, J.T., Bodzęta, A., Stucchi, R., Boumpoutsari, M.M.,
1107 Katrukha, E.A., Altelaar, M., MacGillavry, H.D., Hoogenraad, C.C., 2019. VAP-SCRN1
1108 interaction regulates dynamic endoplasmic reticulum remodeling and presynaptic function.
1109 EMBO J. 38, e101345. doi:10.15252/embj.2018101345
1110 Llano, I., González, J., Caputo, C., Lai, F.A., Blayney, L.M., Tan, Y.P., Marty, A., 2000.
1111 Presynaptic calcium stores underlie large-amplitude miniature IPSCs and spontaneous
1112 calcium transients. Nat. Neurosci. 3, 1256–1265. doi:10.1038/81781
1113 McKinney, R.A., Capogna, M., Dürr, R., Gähwiler, B.H., Thompson, S.M., 1999. Miniature
1114 synaptic events maintain dendritic spines via AMPA receptor activation. Nat. Neurosci. 2,
1115 44–49. doi:10.1038/4548

1116 Meissner, G., 2017. The structural basis of ryanodine receptor ion channel function. J. Gen.
1117 Physiol. 149, 1065–1089. doi:10.1085/jgp.201711878
1118 Miller, B.R., Dorner, J.L., Shou, M., Sari, Y., Barton, S.J., Sengelaub, D.R., Kennedy, R.T.,
1119 Rebec, G.V., 2008. Up-regulation of GLT1 expression increases glutamate uptake and
1120 attenuates the Huntington's disease phenotype in the R6/2 mouse. Neuroscience 153, 329–
1121 337. doi:10.1016/j.neuroscience.2008.02.004
1122 Milnerwood, A.J., Gladding, C.M., Pouladi, M.A., Kaufman, A.M., Hines, R.M., Boyd, J.D., Ko,
1123 R.W.Y., Vasuta, O.C., Graham, R.K., Hayden, M.R., Murphy, T.H., Raymond, L.A., 2010.
1124 Early Increase in Extrasynaptic NMDA Receptor Signaling and Expression Contributes to
1125 Phenotype Onset in Huntington's Disease Mice. Neuron 65, 178–190.
1126 doi:10.1016/j.neuron.2010.01.008
1127 Milnerwood, A.J., Kaufman, A.M., Sepers, M.D., Gladding, C.M., Zhang, L., Wang, L., Fan, J.,
1128 Coquinco, A., Qiao, J.Y., Lee, H., Wang, Y.T., Cynader, M., Raymond, L.A., 2012.
1129 Mitigation of augmented extrasynaptic NMDAR signaling and apoptosis in cortico-striatal
1130 co-cultures from Huntington's disease mice. Neurobiol. Dis. 48, 40–51.
1131 doi:10.1016/j.nbd.2012.05.013
1132 Morton, A.J., Edwardson, J.M., 2001. Progressive depletion of complexin II in a transgenic
1133 mouse model of Huntington's disease. J. Neurochem. 76, 166–172. doi:10.1046/j.1471-
1134 4159.2001.00059.x
1135 Morton, A.J., Faull, R.L., Edwardson, J.M., 2001. Abnormalities in the synaptic vesicle fusion
1136 machinery in Huntington's disease. Brain Res. Bull. 56, 111–117. doi:10.1016/s0361-
1137 9230(01)00611-6
1138 Parsons, M.P., Vanni, M.P., Woodard, C.L., Kang, R., Murphy, T.H., Raymond, L.A., 2016.
1139 Real-time imaging of glutamate clearance reveals normal striatal uptake in Huntington
1140 disease mouse models. Nat Commun 7, 11251. doi:10.1038/ncomms11251
1141 Peled, E.S., Newman, Z.L., Isacoff, E.Y., 2014. Evoked and spontaneous transmission favored
1142 by distinct sets of synapses. Curr. Biol. 24, 484–493. doi:10.1016/j.cub.2014.01.022
1143 Plotkin, J.L., Day, M., Peterson, J.D., Xie, Z., Kress, G.J., Rafalovich, I., Kondapalli, J., Gertler,
1144 T.S., Flajolet, M., Greengard, P., Stavarache, M., Kaplitt, M.G., Rosinski, J., Chan, C.S.,
1145 Surmeier, D.J., 2014. Impaired TrkB Receptor Signaling Underlies Corticostriatal
1146 Dysfunction in Huntington's Disease. Neuron 83, 178–188.
1147 doi:10.1016/j.neuron.2014.05.032
1148 Raymond, L.A., André, V.M., Cepeda, C., Gladding, C.M., Milnerwood, A.J., Levine, M.S.,
1149 2011. Pathophysiology of Huntington's disease: time-dependent alterations in synaptic and
1150 receptor function. Neuroscience 198, 252–273. doi:10.1016/j.neuroscience.2011.08.052
1151 Ross, W.N., 2012. Understanding calcium waves and sparks in central neurons. Nat. Rev.
1152 Neurosci. 13, 157–168. doi:10.1038/nrn3168
1153 Sara, Y., Virmani, T., Deák, F., Liu, X., Kavalali, E.T., 2005. An isolated pool of vesicles
1154 recycles at rest and drives spontaneous neurotransmission. Neuron 45, 563–573.
1155 doi:10.1016/j.neuron.2004.12.056
1156 Sepers, M.D., Smith-Dijak, A., LeDue, J., Kolodziejczyk, K., Mackie, K., Raymond, L.A., 2017.
1157 Endocannabinoid-specific impairment in synaptic plasticity in striatum of Huntington's
1158 disease mouse model. J. Neurosci. 1739–17. doi:10.1523/JNEUROSCI.1739-17.2017
1159 Smith-Dijak, A.I., Nassrallah, W.B., Zhang, L.Y.J., Geva, M., Hayden, M.R., Raymond, L.A.,
1160 2019. Impairment and Restoration of Homeostatic Plasticity in Cultured Cortical Neurons

1161 From a Mouse Model of Huntington Disease. Front Cell Neurosci 13, 209.
1162 doi:10.3389/fncel.2019.00209
1163 Sutton, M.A., Ito, H.T., Cressy, P., Kempf, C., Woo, J.C., Schuman, E.M., 2006. Miniature
1164 neurotransmission stabilizes synaptic function via tonic suppression of local dendritic protein
1165 synthesis. Cell 125, 785–799. doi:10.1016/j.cell.2006.03.040
1166 Sutton, M.A., Taylor, A.M., Ito, H.T., Pham, A., Schuman, E.M., 2007. Postsynaptic decoding of
1167 neural activity: eEF2 as a biochemical sensor coupling miniature synaptic transmission to
1168 local protein synthesis. Neuron 55, 648–661. doi:10.1016/j.neuron.2007.07.030
1169 Suzuki, M., Nagai, Y., Wada, K., Koike, T., 2012. Calcium leak through ryanodine receptor is
1170 involved in neuronal death induced by mutant huntingtin. Biochem. Biophys. Res. Commun.
1171 429, 18–23. doi:10.1016/j.bbrc.2012.10.107
1172 Tang, T.-S., Tu, H., Chan, E.Y.W., Maximov, A., Wang, Z., Wellington, C.L., Hayden, M.R.,
1173 Bezprozvanny, I., 2003. Huntingtin and huntingtin-associated protein 1 influence neuronal
1174 calcium signaling mediated by inositol-(1,4,5) triphosphate receptor type 1. Neuron 39, 227–
1175 239.
1176 Tang, T.S., Guo, C., Wang, H., Chen, X., Bezprozvanny, I., 2009. Neuroprotective Effects of
1177 Inositol 1,4,5-Trisphosphate Receptor C-Terminal Fragment in a Huntington's Disease
1178 Mouse Model. Journal of Neuroscience 29, 1257–1266. doi:10.1523/JNEUROSCI.4411-
1179 08.2009
1180 Tyebji, S., Hannan, A.J., 2017. Synaptopathic mechanisms of neurodegeneration and dementia:
1181 Insights from Huntington's disease. Prog. Neurobiol. 153, 18–45.
1182 doi:10.1016/j.pneurobio.2017.03.008
1183 van de Vrede, Y., Fossier, P., Baux, G., Joels, M., Chameau, P., 2007. Control of IsAHP in
1184 mouse hippocampus CA1 pyramidal neurons by RyR3-mediated calcium-induced calcium
1185 release. Pflugers Arch. 455, 297–308. doi:10.1007/s00424-007-0277-4
1186 Vonsattel, J.P., Myers, R.H., Stevens, T.J., Ferrante, R.J., Bird, E.D., Richardson, E.P., 1985.
1187 Neuropathological classification of Huntington's disease. J. Neuropathol. Exp. Neurol. 44,
1188 559–577.
1189 Wang, R., Reddy, P.H., 2017. Role of Glutamate and NMDA Receptors in Alzheimer's Disease.
1190 J. Alzheimers Dis. 57, 1041–1048. doi:10.3233/JAD-160763
1191 Wang, Y., DelRosso, N.V., Vaidyanathan, T.V., Cahill, M.K., Reitman, M.E., Pittolo, S., Mi, X.,
1192 Yu, G., Poskanzer, K.E., 2019. Accurate quantification of astrocyte and neurotransmitter
1193 fluorescence dynamics for single-cell and population-level physiology. Nat. Neurosci. 22,
1194 1936–1944. doi:10.1038/s41593-019-0492-2
1195 Xu, J., Pang, Z.P., Shin, O.-H., Südhof, T.C., 2009. Synaptotagmin-1 functions as a Ca2+ sensor
1196 for spontaneous release. Nat. Neurosci. 12, 759–766. doi:10.1038/nn.2320
1197 Zeron, M.M., Hansson, O., Chen, N., Wellington, C.L., Leavitt, B.R., Brundin, P., Hayden,
1198 M.R., Raymond, L.A., 2002. Increased Sensitivity to N-Methyl-D-Aspartate Receptor-
1199 Mediated Excitotoxicity in a Mouse Model of Huntington's Disease. Neuron 33, 849–860.
1200 doi:10.1016/S0896-6273(02)00615-3
1201

Figure 1:

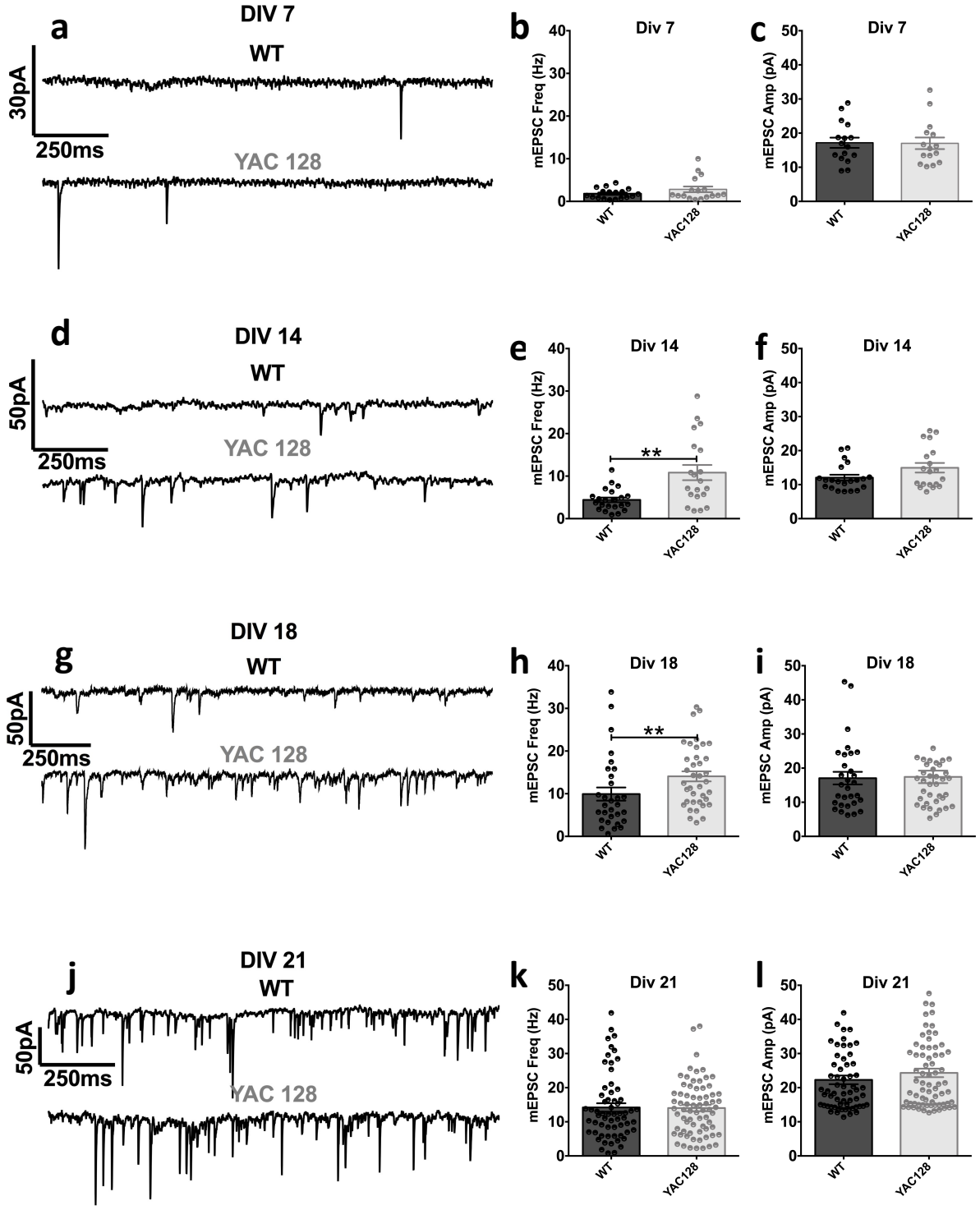
a
DIV 7
WT
30pA
250ms
YAC 128
b
Div 7
mEPSC Freq (Hz)
WT
YAC128
c
Div 7
mEPSC Amp (pA)
WT
YAC128
d
DIV 14
WT
50pA
250ms
YAC 128
e
Div 14
mEPSC Freq (Hz)
**
WT
YAC128
f
Div 14
mEPSC Amp (pA)
WT
YAC128
g
DIV 18
WT
50pA
250ms
YAC 128
h
Div 18
mEPSC Freq (Hz)
**
WT
YAC128
i
Div 18
mEPSC Amp (pA)
WT
YAC128
j
DIV 21
WT
50pA
250ms
YAC 128
k
Div 21
mEPSC Freq (Hz)
WT
YAC128
l
Div 21
mEPSC Amp (pA)
WT
YAC128

Supplemental Figure 1:

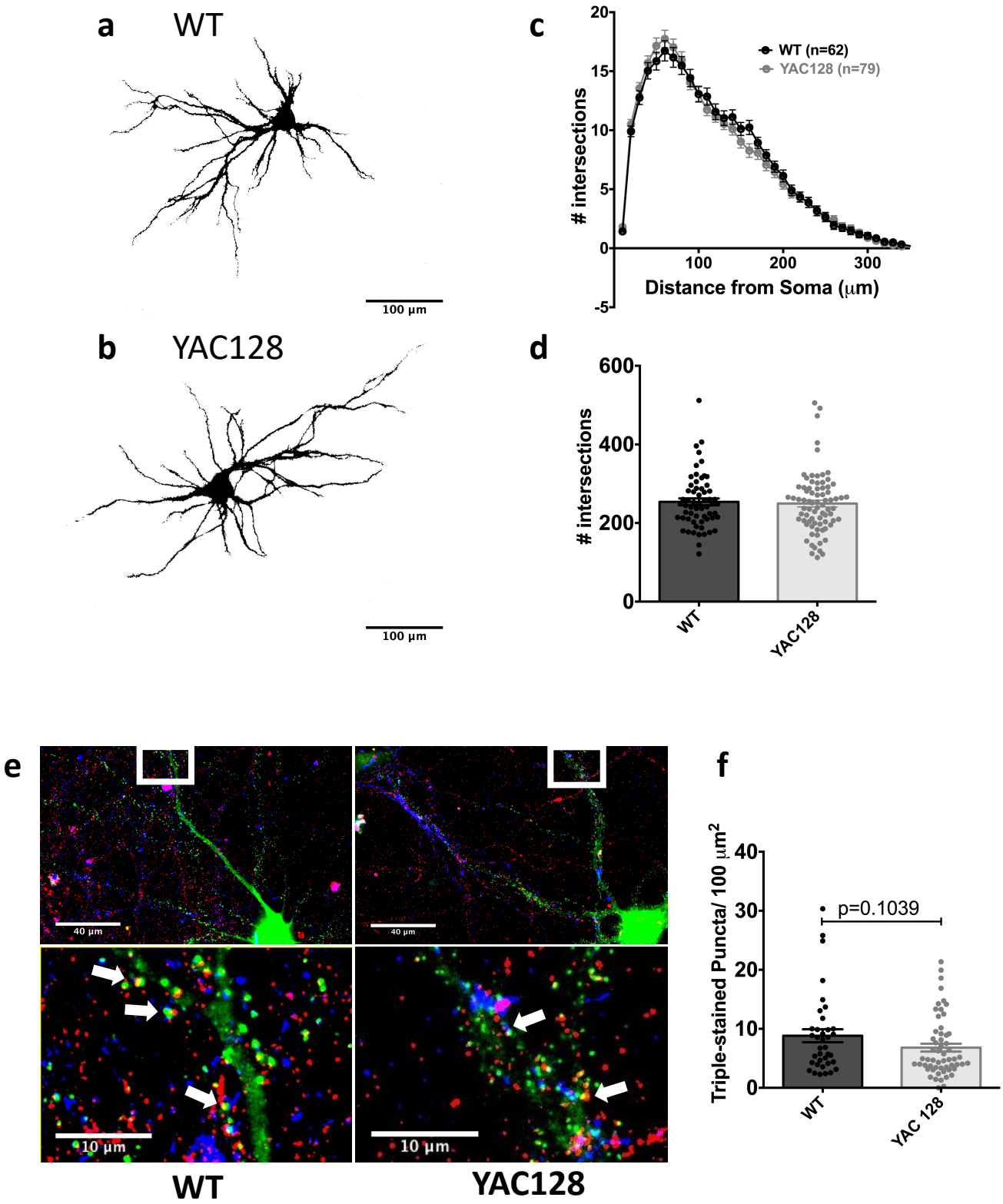

Figure 2:

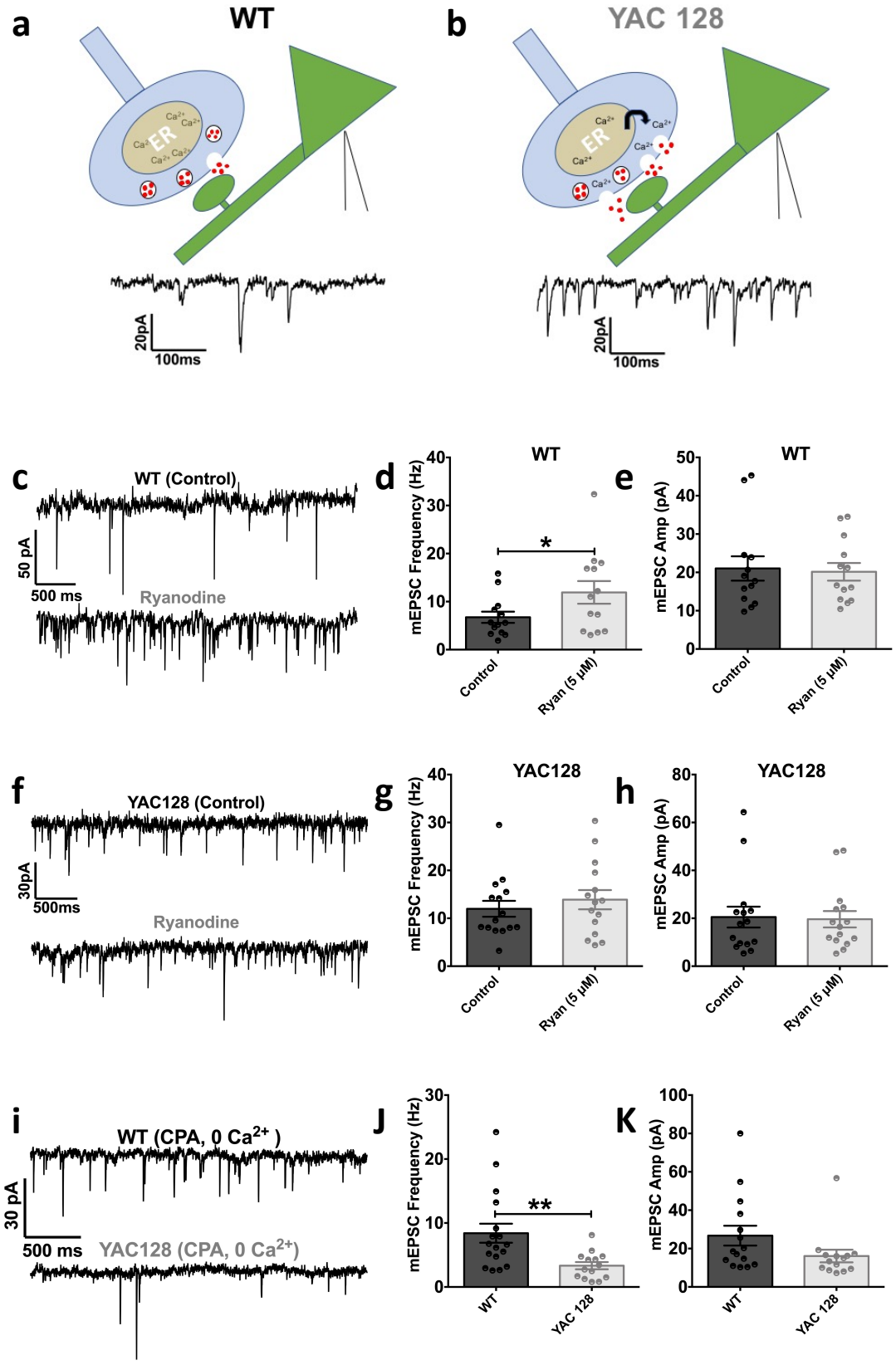
a
WT
ER
20pA
100ms
b
YAC 128
ER
20pA
100ms
c
WT (Control)
50 pA
500 ms
Ryanodine
d
WT
mEPSC Frequency (Hz)
*
Control
Ryan (5 μM)
e
WT
mEPSC Amp (pA)
Control
Ryan (5 μM)
f
YAC128 (Control)
30pA
500ms
Ryanodine
g
YAC128
mEPSC Frequency (Hz)
Control
Ryan (5 μM)
h
YAC128
mEPSC Amp (pA)
Control
Ryan (5 μM)
i
WT (CPA, 0 Ca2+)
30 pA
500 ms
YAC128 (CPA, 0 Ca2+)
J
mEPSC Frequency (Hz)
**
WT
YAC 128
K
mEPSC Amp (pA)
WT
YAC 128

Supplemental Figure 2:

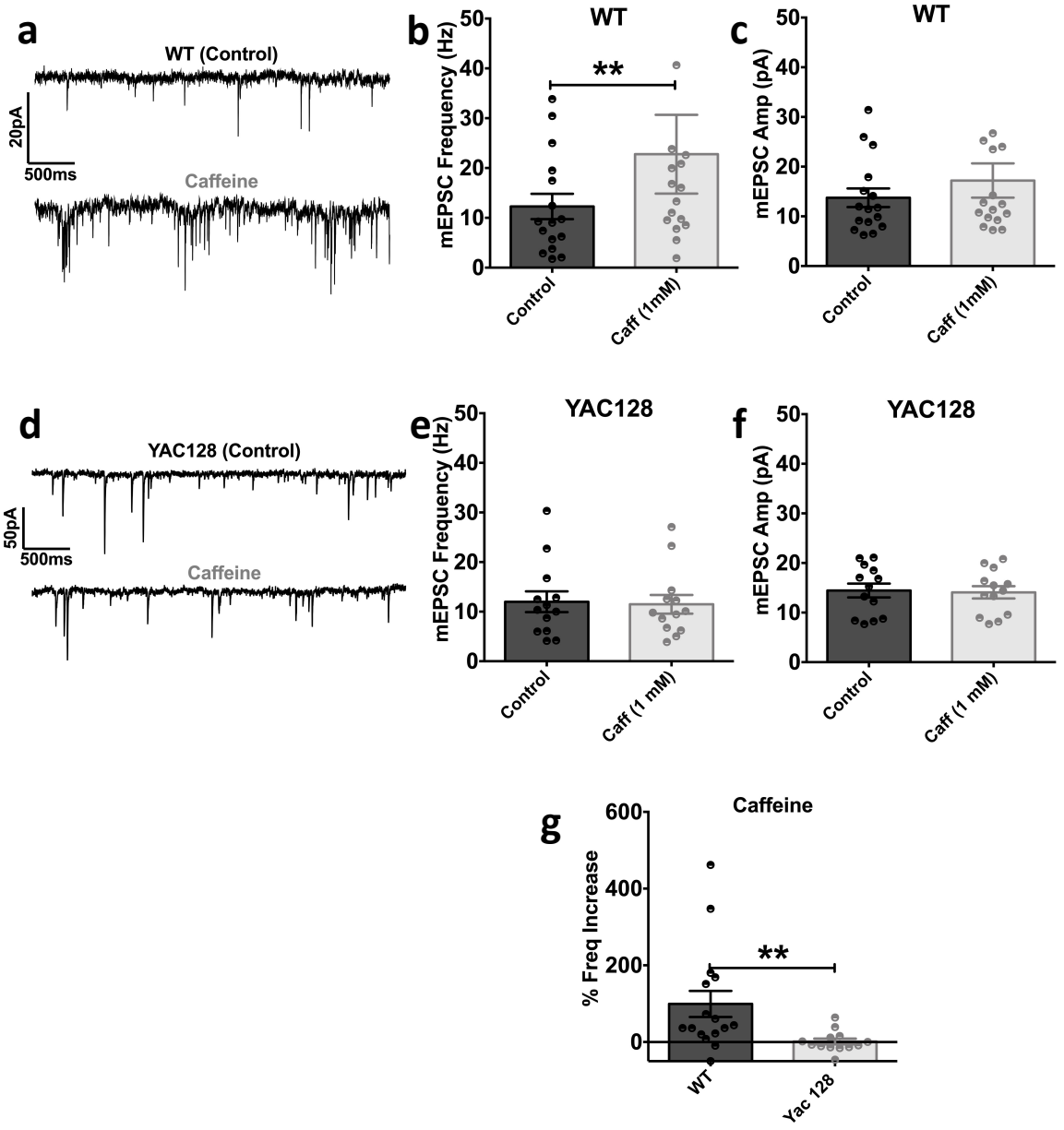

Figure 3:

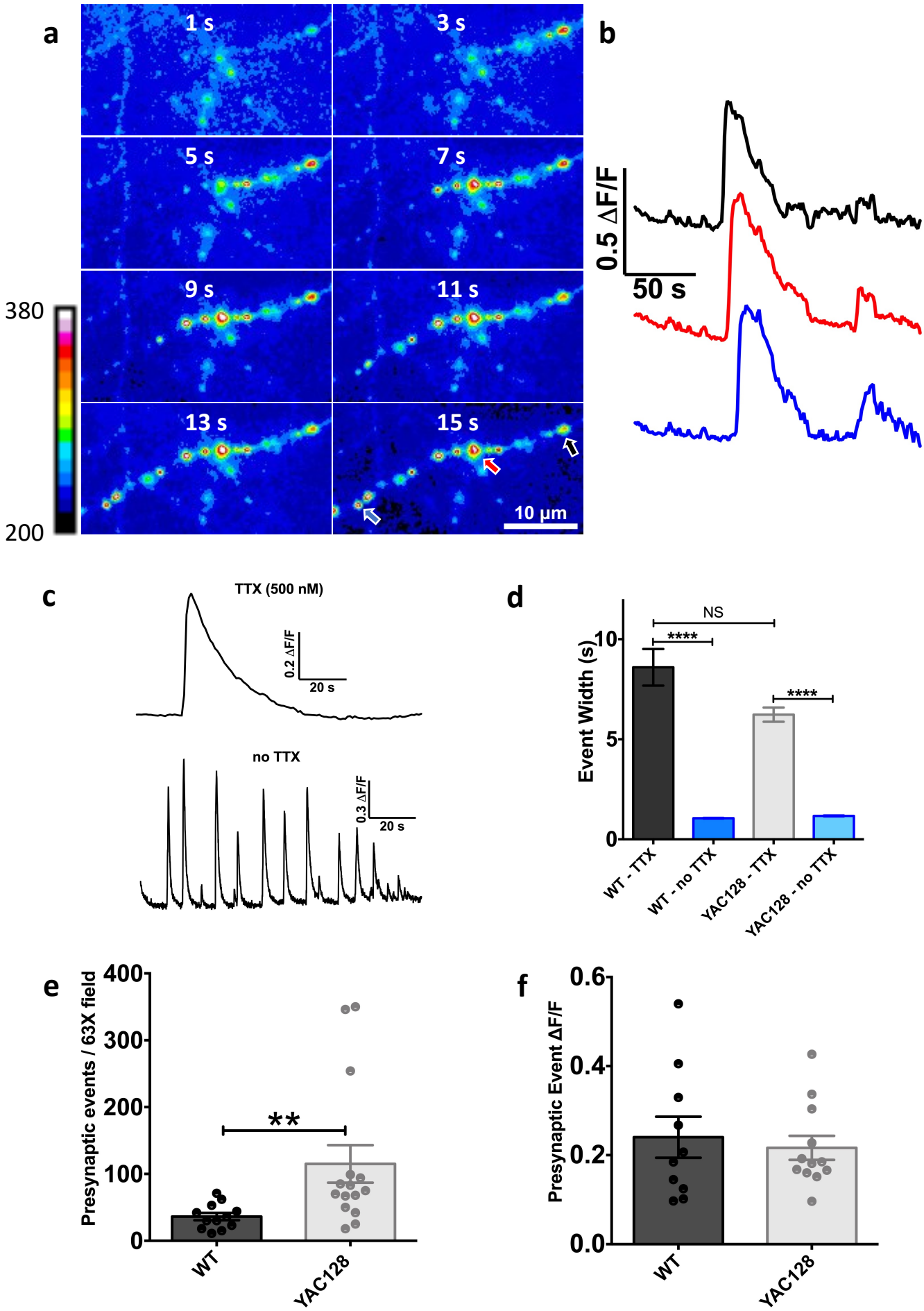
a
1 s
3 s
5 s
7 s
9 s
11 s
13 s
15 s
10 µm
380
200
b
0.5 ΔF/F
50 s
c
TTX (500 nM)
0.2 ΔF/F
20 s
no TTX
0.3 ΔF/F
20 s
d
Event Width (s)
NS
****
****
WT - TTX
WT - no TTX
YAC128 - TTX
YAC128 - no TTX
e
Presynaptic events / 63X field
**
WT
YAC128
f
Presynaptic Event ΔF/F
WT
YAC128

Figure 4:

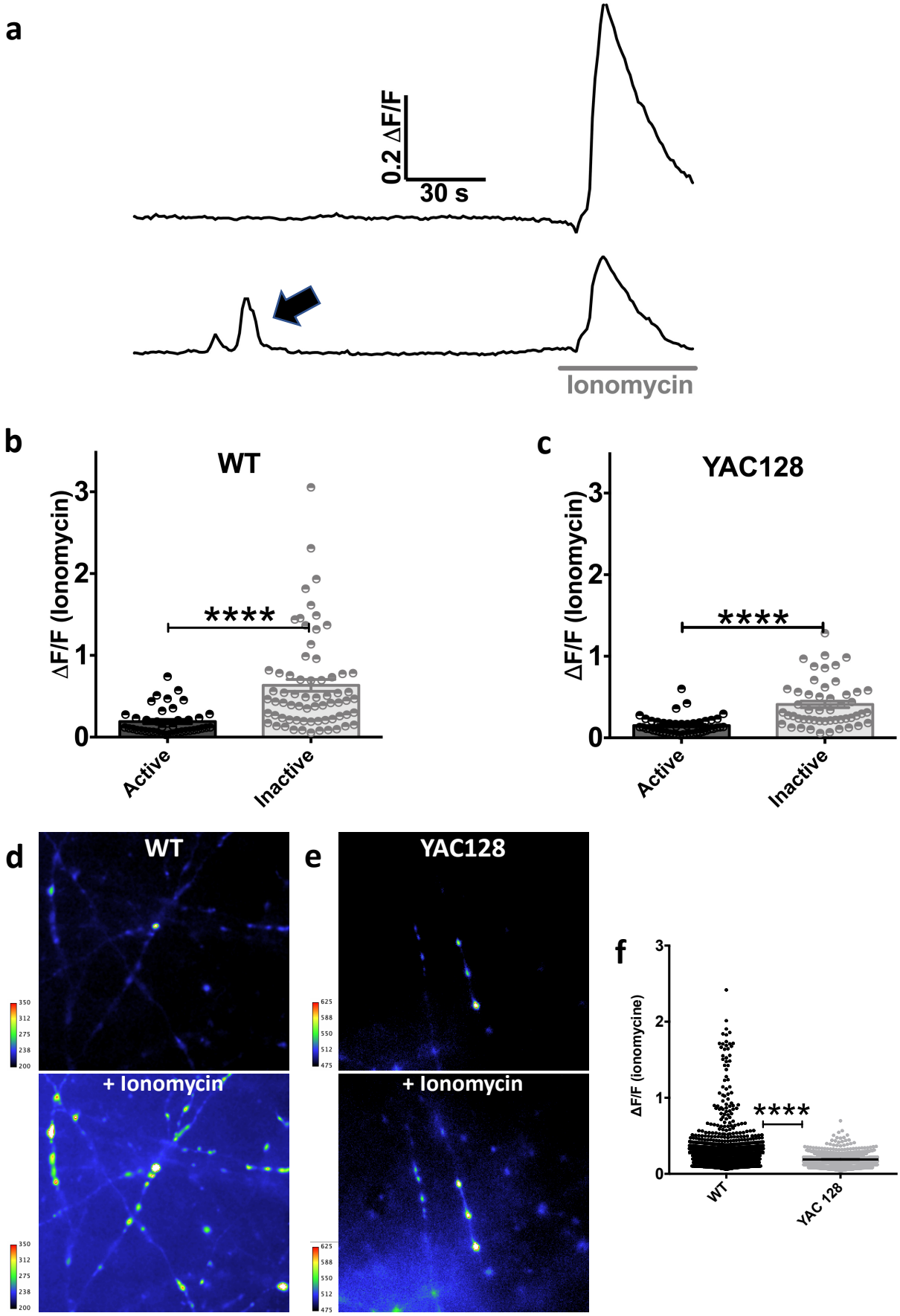
a
0.2 ΔF/F
30 s
Ionomycin
b
WT
ΔF/F (Ionomycin)
****
Active
Inactive
c
YAC128
ΔF/F (Ionomycin)
****
Active
Inactive
d
WT
+ Ionomycin
e
YAC128
+ Ionomycin
f
ΔF/F (ionomycine)
****
WT
YAC 128

Figure 5:

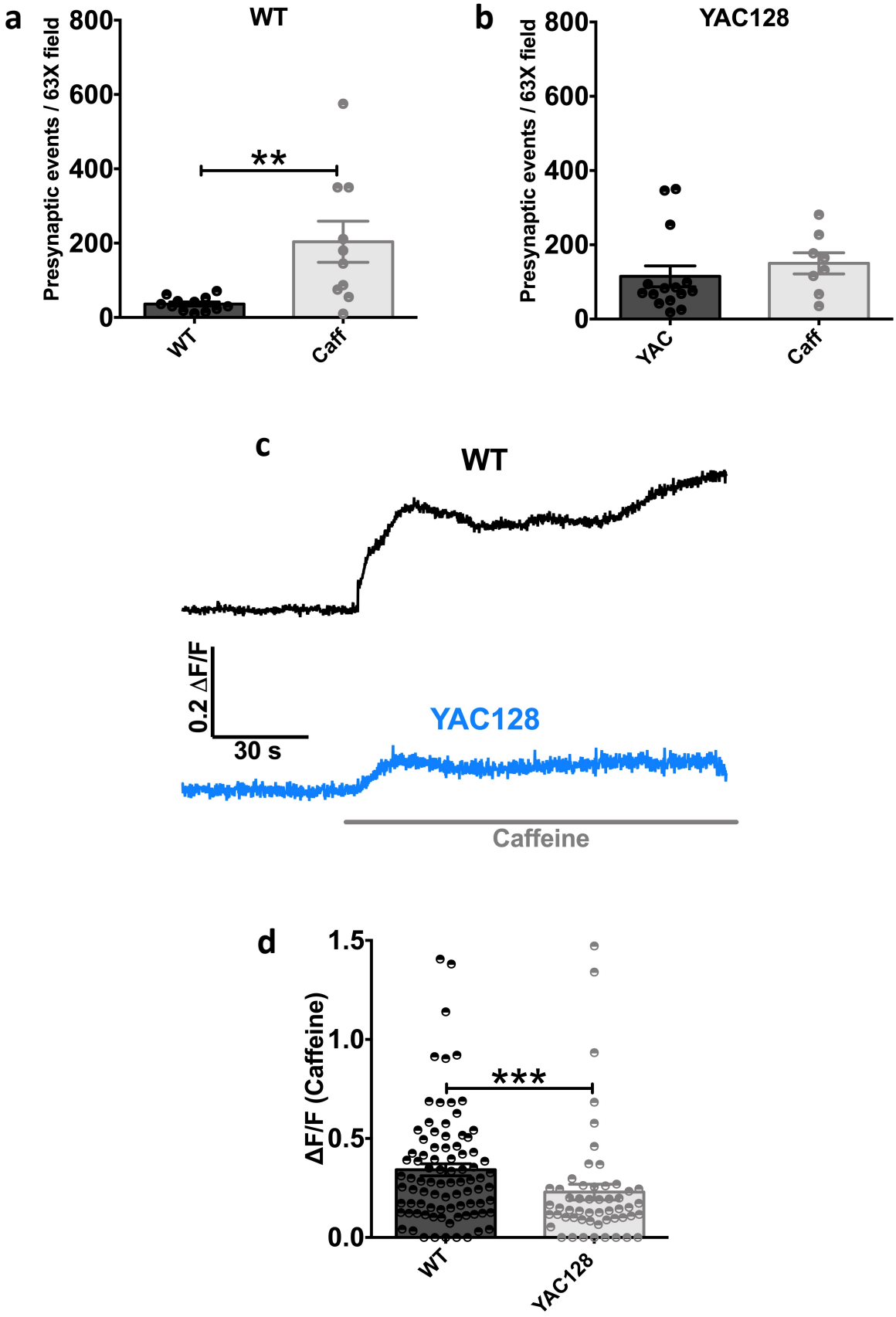
a
WT
Presynaptic events / 63X field
800
600
400
200
0
**
WT
Caff
b
YAC128
Presynaptic events / 63X field
800
600
400
200
0
YAC
Caff
c
WT
0.2 ΔF/F
30 s
YAC128
Caffeine
d
ΔF/F (Caffeine)
1.5
1.0
0.5
0.0
***
WT
YAC128

Figure 6:

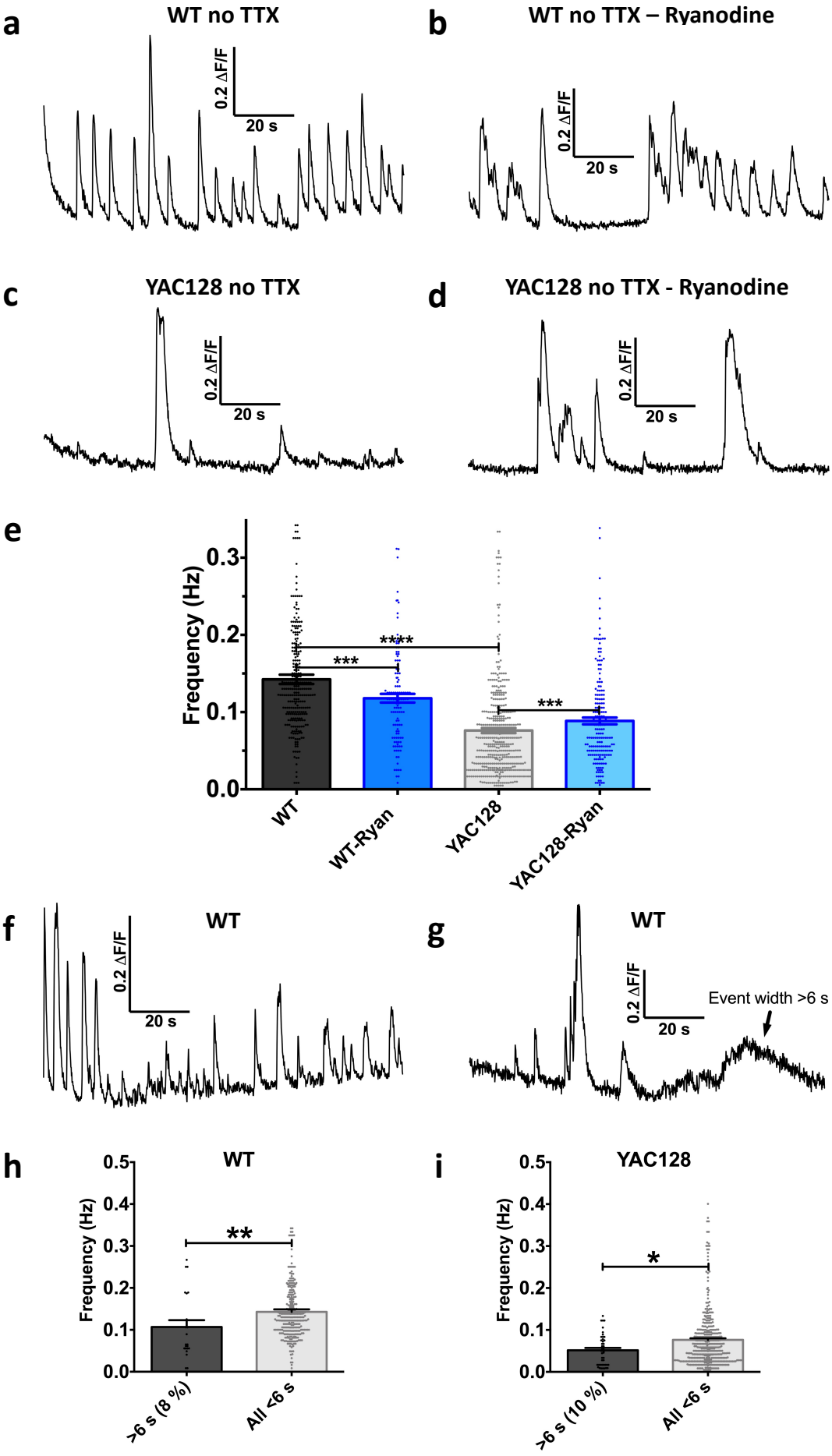
a
WT no TTX
0.2 ΔF/F
20 s
b
WT no TTX – Ryanodine
0.2 ΔF/F
20 s
c
YAC128 no TTX
0.2 ΔF/F
20 s
d
YAC128 no TTX - Ryanodine
0.2 ΔF/F
20 s
e
Frequency (Hz)
0.0
0.1
0.2
0.3
****
***
***
WT
WT-Ryan
YAC128
YAC128-Ryan
f
WT
0.2 ΔF/F
20 s
g
WT
0.2 ΔF/F
20 s
Event width >6 s
h
WT
Frequency (Hz)
0.0
0.1
0.2
0.3
0.4
0.5
**
>6 s (8 %)
All <6 s
i
YAC128
Frequency (Hz)
0.0
0.1
0.2
0.3
0.4
0.5
*
>6 s (10 %)
All <6 s

Figure 7:

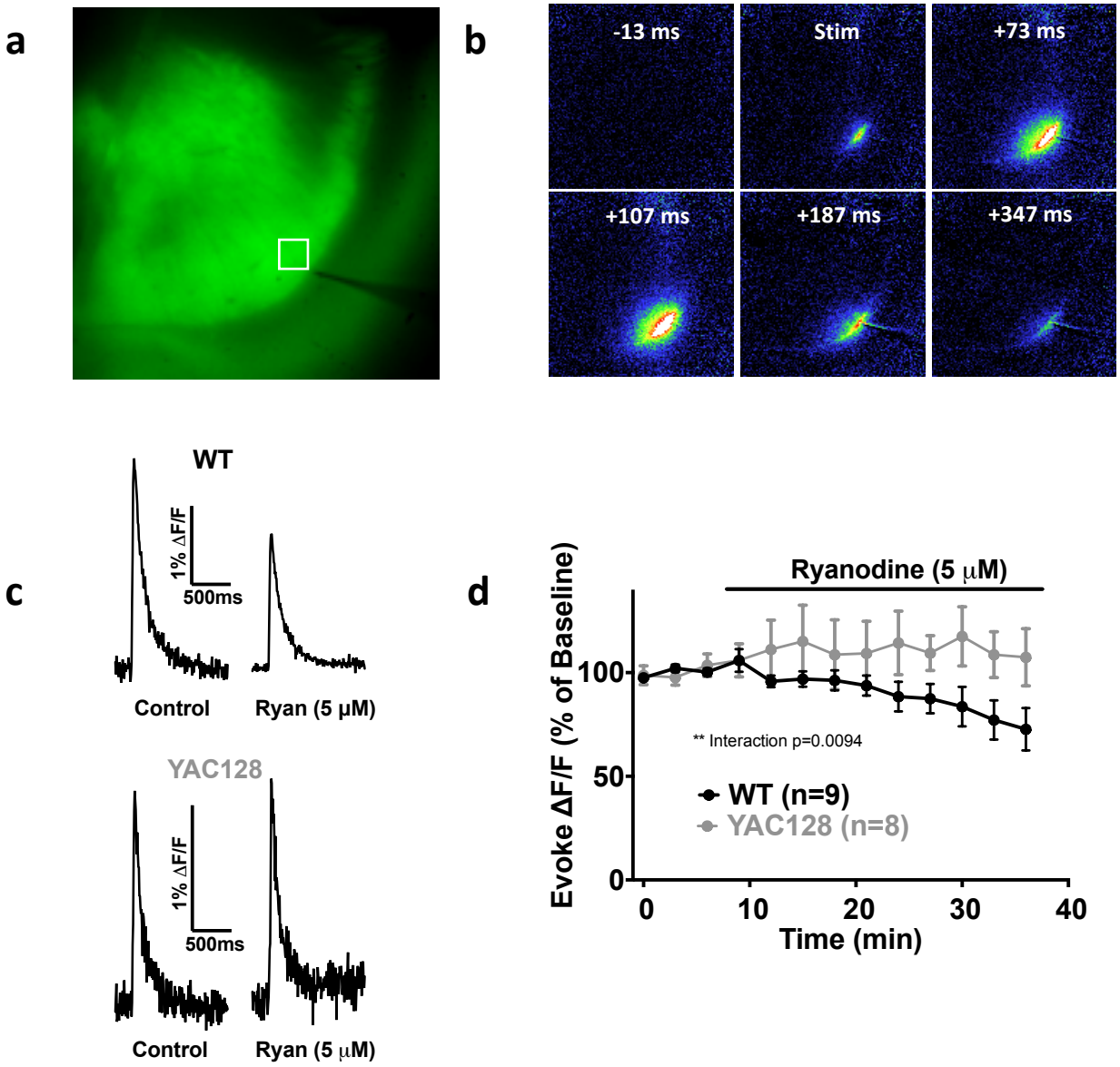
a
b
-13 ms
Stim
+73 ms
+107 ms
+187 ms
+347 ms
c
WT
1% ΔF/F
500ms
Control
Ryan (5 μM)
YAC128
1% ΔF/F
500ms
Control
Ryan (5 μM)
d
Ryanodine (5 μM)
Evoke ΔF/F (% of Baseline)
100
50
0
** Interaction p=0.0094
WT (n=9)
YAC128 (n=8)
0
10
20
30
40
Time (min)